

# Final Technical Report

## Recovery Act: Online Nonintrusive Condition Monitoring and Fault Detection for Wind Turbines

Award Number: DE-EE0001366

Project Period: 11:09–02:12

Principal Investigator:

Wei Qiao

Tel: (402) 472-9619

E-mail: [wqiao@engr.unl.edu](mailto:wqiao@engr.unl.edu)

Recipient Organization:

Board of Regents, Univ. of Nebraska, Univ. of Nebraska-Lincoln

1400 R Street

Lincoln, NE 68588

May 29, 2012

### **Acknowledgment**

This report is based upon work supported by the U. S. Department of Energy under Award No. DE-EE0001366.

### **Disclaimer**

Any findings, opinions, and conclusions or recommendations expressed in this report are those of the author and do not necessarily reflect the views of the Department of Energy.

# TABLE OF CONTENTS

LIST OF ACRONYMS .....	iii
LIST OF FIGURES .....	iv
LIST OF TABLES .....	vii
EXECUTIVE SUMMARY .....	1
1 INTRODUCTION .....	3
2 BACKGROUND .....	7
2.1 Motivation.....	7
2.2 Project Goal and Objectives.....	8
2.3 Qualifications and Experience of the Project Team .....	9
3 CURRENT-BASED WIND TURBINE CMFD TECHNOLOGIES .....	10
3.1 Modulation of Current Signals by a Wind Turbine Fault.....	10
3.2 Current Demodulation .....	13
3.2.1 Frequency Demodulation.....	13
3.2.2 Amplitude Demodulation.....	14
3.2.3 Benefits of Using Current Demodulation .....	14
3.3 1P-Invariant PSD Method.....	14
3.4 Wavelet Filter.....	17
3.5 Impulse Detection .....	18
4 SIMULATION AND EXPERIMENTAL VALIDATION PLATFORMS.....	20
4.1 Simulation Validation Platform .....	20
4.1.1 WTG Model.....	20
4.2.2 Wind Speed Data .....	21
4.2 Experimental Validation Platform .....	22
5 WIND TURBINE IMBALANCE FAULT DETECTION .....	24
5.1 The Characteristic Frequencies of Imbalance Faults .....	24
5.2 Simulation Study of Imbalance Fault Detection.....	26
5.3 Experimental Study of Imbalance Fault Detection.....	29
5.3.1 Detection of Blade Imbalance.....	29
5.3.2 Detection of Bent Blades .....	35

5.3.3	Detection of Aged Blade.....	38
5.3.4	Detection of Blade Defects.....	40
5.3.5	Detection of Generator Magnet Damage.....	42
6	WIND TURBINE BEARING FAULT DETECTION.....	44
6.1	The Characteristic Frequencies of Single-Point Bearing Faults.....	44
6.1.1	Types of Single-Point Bearing Faults.....	44
6.1.2	Bearing Fault Signatures in Stator Current Signals.....	45
6.2	Single-Point Bearing Fault Detection.....	46
6.2.1	WTG with Healthy Bearings.....	46
6.2.2	WTG with a Bearing Cage Broken Fault.....	48
6.2.3	WTG with an Out-Race Fault.....	52
6.3	Incipient Bearing Fault Detection.....	54
7	ACCOMPLISHMENTS.....	56
7.1	Publications.....	56
7.2	Presentations.....	57
7.3	Patent.....	57
8	CONCLUSIONS.....	58
9	RECOMMENDATIONS.....	60
	REFERENCES.....	61

## LIST OF ACRONYMS

CMFD	condition monitoring and fault detection
DFIG	doubly fed induction generator
DWT	discrete wavelet transform
FAST	Fatigue, Aerodynamics, Structures, and Turbulence
NREL	National Renewable Energy Laboratory
O&M	operation and maintenance
PLL	phase lock loop
PI	principal investigator
PMSG	permanent magnet synchronous generator
PSD	power spectrum density
R&D	research and development
SNR	signal-to-noise ratio
UNL	University of Nebraska-Lincoln
WTG	wind turbine generator

## LIST OF FIGURES

1.1	The proposed technologies for CMFD of a wind turbine .....	5
1.2	Overall framework of the proposed current-based wind turbine CMFD technologies .....	5
3.1	Schematic diagram of a PLL for signal frequency demodulation .....	13
3.2	Schematic diagram of the 1P-invariant PSD method .....	16
3.3	Schematic diagram of the wavelet filter method .....	17
3.4	Schematic diagram of the impulse detection method .....	19
4.1	Structure of the simulation validation platform .....	20
4.2	The wind tunnel with a testing WTG in the UNL's Power & Energy Systems laboratory	21
4.3	Sensing and data acquisition system for the testing WTGs .....	22
5.1	Effect of blade imbalance of a wind turbine .....	25
5.2	Effect of an aerodynamic asymmetry of a wind turbine caused by wind shear .....	25
5.3	Comparison of the 1P-invariant PSD of the estimated shaft rotating frequency for the blade imbalance scenarios against the baseline case in a wide frequency range .....	27
5.4	Comparison of the 1P-invariant PSD of the estimated shaft rotating frequency for the blade imbalance scenarios against the baseline case in a frequency range around 1P .....	27
5.5	Comparison of the 1P-invariant PSD of the estimated shaft rotating frequency for the aerodynamic asymmetry scenarios against the baseline case in a wide frequency range .....	28
5.6	Comparison of the 1P-invariant PSD of the estimated shaft rotating frequency for the aerodynamic asymmetry scenarios against the baseline case in a frequency range around 1P .....	28
5.7	Comparison of the 1P-invariant PSD of the estimated shaft rotating frequency for the aerodynamic asymmetry scenarios against the baseline case in a frequency range around 2P .....	29
5.8	A blade with an additional mass to create a blade imbalance fault .....	30
5.9	Comparison of the 1P-invariant PSD of the current signal for the blade imbalance scenarios against the baseline case in a wide frequency range .....	30
5.10	Comparison of the 1P-invariant PSD of the current signal for the blade imbalance scenarios against the baseline case around 50 Hz and 70 Hz .....	31
5.11	Comparison of the 1P-invariant PSD of the estimated shaft rotating frequency for the blade imbalance scenarios against the baseline case in a wide frequency range .....	33
5.12	Comparison of the 1P-invariant PSD of the estimated shaft rotating frequency for the blade imbalance scenarios against the baseline case in a frequency range around 1P .....	33
5.13	Comparison of the 1P-invariant PSD of the vibration signal for the blade imbalance scenarios against the baseline case in a wide frequency range .....	34
5.14	Comparison of the 1P-invariant PSD of the vibration signal for the blade imbalance scenarios against the baseline case in a frequency range around 1P .....	34

5.15	A blade bended flapwise or edgewise.....	35
5.16	Comparison of the 1P-invariant PSD of the estimated shaft rotating frequency for the edgewise bent blade scenarios against the baseline case in a wide frequency range .....	36
5.17	Comparison of the 1P-invariant PSD of the estimated shaft rotating frequency for the edgewise bent blade scenarios against the baseline case in a frequency range around 1P	36
5.18	A blade of the Air Breeze wind turbine bended forward (left) and backward (right) .....	37
5.19	Comparison of the 1P-invariant PSD of the estimated shaft rotating frequency for the flapwise bent blade scenarios against the baseline case in a frequency range around 1P	37
5.20	Comparison of the 1P-invariant PSD of the vibration signal for the flapwise bent blade scenarios against the baseline case in a frequency range around 1P .....	38
5.21	Comparison of the aged blade with a new blade .....	38
5.22	Comparison of the 1P-invariant PSD of the estimated shaft rotating frequency for the aged blade case against the baseline case in a frequency range around 1P .....	39
5.23	Comparison of the 1P-invariant PSD of the vibration signal for the aged blade case against the baseline case in a frequency range around 1P .....	39
5.24	Two defected blades used for experiments.....	40
5.25	Comparison of the 1P-invariant PSD of the estimated shaft rotating frequency for the blade defect cases against the baseline case in a frequency range around 1P .....	41
5.26	Comparison of the 1P-invariant PSD of the vibration signal for the blade defect cases against the baseline case in a frequency range around 1P .....	41
5.27	A rotor with a damaged magnet of the generator of an Air Breeze wind turbine.....	42
5.28	Comparison of the 1P-invariant PSD of the estimated shaft rotating frequency for the magnet damage case against the baseline case in a frequency range around 1P .....	42
5.29	Comparison of the 1P-invariant PSD of the vibration signal for the magnet damage case against the baseline case in a frequency range around 1P .....	43
6.1	Schematic diagram of a ball bearing.....	45
6.2	The testing bearing and WTG.....	46
6.3	The 1P-invariant PSD of the frequency demodulated signal of the stator current in the healthy bearing case.....	47
6.4	The 1P-invariant PSD of the amplitude demodulated signal of the stator current in the healthy bearing case.....	47
6.5	Testing bearing: (a) is healthy before experiment and (b) with broken cage after experiment.....	48
6.6	Comparison of the 1P-invariant PSDs of the processed shaft rotating frequency signals estimated from the first and the last stator current records.....	49
6.7	Locally normalized PSD and threshold generated by the impulse detection method for the bearing with cage fault.....	49
6.8	Amplitudes of the locally normalized PSD at the bearing cage fault characteristic frequency of 4 Hz during the 25-hour experiment.....	50

6.9	The standard PSD of the stator current measurements in the bearing fault case.....	51
6.10	The 1P-invariant PSD of the stator current measurements in the bearing fault case.....	51
6.11	The testing bearing with an outer-race fault .....	52
6.12	Comparison of the 1P-invariant PSDs of the estimated shaft rotating frequency signals for the WTG with a bearing outer-race fault against that with a healthy bearing .....	53
6.13	Locally normalized PSD and threshold generated by the impulse detection method for the bearing with an outer-race fault .....	53
6.14	The results of the wavelet-filtered stator current .....	55

**LIST OF TABLES**

6.1 Characteristic frequencies of single-point bearing faults in WTG current signals.....45

## EXECUTIVE SUMMARY

The penetration of wind power has increased greatly over the last decade in the United States and across the world. The U.S. wind power industry installed 1,118 MW of new capacity in the first quarter of 2011 alone and entered the second quarter with another 5,600 MW under construction [1]. By 2030, wind energy is expected to provide 20% of the U.S. electricity needs [2]. As the number of wind turbines continues to grow, the need for effective condition monitoring and fault detection (CMFD) systems becomes increasingly important [3]. Online CMFD is an effective means of not only improving the reliability, capacity factor, and lifetime, but it also reduces the downtime, energy loss, and operation and maintenance (O&M) of wind turbines.

The goal of this project is to develop novel online nonintrusive CMFD technologies for wind turbines. The proposed technologies use only the current measurements that have been used by the control and protection system of a wind turbine generator (WTG); no additional sensors or data acquisition devices are needed. Current signals are reliable and easily accessible from the ground without intruding on the wind turbine generators (WTGs) that are situated on high towers and installed in remote areas. Therefore, current-based CMFD techniques have great economic benefits and the potential to be adopted by the wind energy industry. Specifically, the following objectives and results have been achieved in this project.

- Analyzed the effects of faults in a WTG on the generator currents of the WTG operating at variable rotating speed conditions from the perspective of amplitude and frequency modulations of the current measurements
- Developed effective amplitude and frequency demodulation methods for appropriate signal conditioning of the current measurements to improve the accuracy and reliability of wind turbine CMFD.
- Developed a 1P-invariant power spectrum density (PSD) method for effective signature extraction of wind turbine faults with characteristic frequencies in the current or current demodulated signals, where 1P stands for the shaft rotating frequency of a WTG.
- Developed a wavelet filter for effective signature extraction of wind turbine faults without characteristic frequencies in the current or current demodulated signals.
- Developed an effective adaptive noise cancellation method as an alternative to the wavelet filter method for signature extraction of wind turbine faults without characteristic frequencies in the current or current demodulated signals.
- Developed a statistical analysis-based impulse detection method for effective fault signature extraction and evaluation of WTGs based on the 1P-invariant PSD of the current or current demodulated signals.
- Validated the proposed current-based wind turbine CMFD technologies through extensive computer simulations and experiments for small direct-drive WTGs without gearboxes.

- Showed, through extensive experiments for small direct-drive WTGs, that the performance of the proposed current-based wind turbine CMFD technologies is comparable to traditional vibration-based methods.

The proposed technologies have been successfully applied for detection of major failures in blades, shafts, bearings, and generators of small direct-drive WTGs. The proposed technologies can be easily integrated into existing wind turbine control, protection, and monitoring systems and can be implemented remotely from the wind turbines being monitored. The proposed technologies provide an alternative to vibration-sensor-based CMFD. This will reduce the cost and hardware complexity of wind turbine CMFD systems. The proposed technologies can also be combined with vibration-sensor-based methods to improve the accuracy and reliability of wind turbine CMFD systems. When there are problems with sensors, the proposed technologies will ensure proper CMFD for the wind turbines, including their sensing systems.

In conclusion, the proposed technologies offer an effective means to achieve condition-based smart maintenance for wind turbines and have a great potential to be adopted by the wind energy industry due to their almost no-cost, nonintrusive features.

Although only validated for small direct-drive wind turbines without gearboxes, the proposed technologies are also applicable for CMFD of large-size wind turbines with and without gearboxes. However, additional investigations are recommended in order to apply the proposed technologies to those large-size wind turbines.

# 1. INTRODUCTION

Wind turbines are usually situated on high towers, installed in remote rural areas, distributed over large geographic regions, subject to harsh environments, and experience relatively high failure rates. It was reported [4], [5] that the maintenance costs for onshore and offshore wind turbines are in the order of 10-15% and 20-35%, respectively, of the total cost of the electricity generated. To make wind energy competitive with traditional forms of energy sources for electricity generation, it is necessary to reduce the maintenance costs and improve the reliability of wind turbines. The most efficient way to achieve this objective would be to perform maintenance based on online CMFD.

Most existing methods for wind turbine CMFD require additional mechanical sensors and data acquisition devices to implement [5]. The most commonly used sensors are vibration sensors, such as accelerometers. These sensors are usually mounted on the surface or buried in the body of WTG components, which are situated on high towers and are difficult to access during WTG operation. Moreover, the sensors and data acquisition devices are inevitably subject to failure, which could cause additional problems with system reliability and additional O&M costs.

Compared to traditional methods using vibration or other types of sensors, current-based wind turbine CMFD techniques are advantageous in terms of cost, implementation, and system reliability. However, there are challenges in using current signals for wind turbine CMFD. First, the dominant components of a current signal acquired from a WTG in the frequency domain are the fundamental-frequency component and its harmonics. Therefore, the useful information (i.e., the fault signature) in current signals for wind turbine fault detection usually has a low signal-to-noise ratio (SNR), which makes fault detection difficult. Appropriate signal processing methods are needed to properly extract fault signatures for effective fault detection of wind turbines.

Another issue associated with using current signals for wind turbine CMFD is how a fault in a WTG will affect the current signal acquired from the WTG, and what is the best way to use the current signal for wind turbine CMFD. The findings of this project have revealed that a WTG fault would induce a vibration and, therefore, a shaft torque variation of the WTG at certain frequencies. Such a shaft torque variation will modulate the amplitude and frequency of the current signals of the WTG [7], [8]. In some wind turbine faults, the induced shaft torque variation may have overlaps with the dominant components in the frequency spectra of the current signals. Therefore, the useful information related to faults is masked by the dominant components and cannot be extracted directly from the current spectra. Appropriate demodulation methods are, therefore, needed to separate the useful information related to the faults from the dominant components in the current signals to facilitate the extraction of fault signatures from the current signals. The current frequency and amplitude demodulation methods developed in this project are based on a phase lock loop (PLL) technique and a square law, respectively.

According to the fault signatures in the signals used for CMFD, wind turbine faults can be classified into two categories: the faults with one or more characteristic frequencies (called Type 1 faults), such as single-point bearing fault, rotor/blade imbalance, and aerodynamic asymmetries [9], [10], and the faults without characteristic frequencies (called Type 2 faults), such as incipient

bearing faults [11]. For Type 1 faults, the characteristic frequencies depend on the shaft rotating frequency of the WTG, which is known as the 1P frequency [12]. As mentioned in [13], since the 1P frequency of a WTG usually varies with wind speed, it is a problem to extract the fault signatures from the nonstationary current signals of the WTG using traditional frequency spectrum analysis methods. To overcome the limitations of the traditional frequency spectrum analysis methods, a 1P-invariant PSD method [9] has been developed in this project for effective extraction of fault signatures from nonstationary current signals of WTGs operating in variable-speed conditions. In the proposed 1P-invariant PSD method, the current signal, current frequency demodulated signal, or current amplitude demodulated signal is processed by using appropriate up-sampling and variable-rate down-sampling algorithms. Consequently, the variable characteristic frequencies of wind turbine faults in the spectra of these signals are converted to constant values. Therefore, the signatures of wind turbine faults can be clearly identified from the PSD analysis of the processed signals.

On the other hand, since the Type 2 faults in WTGs do not have a characteristic frequency, they cannot be detected by using frequency-domain spectrum analysis methods. Moreover, the major challenge of low SNR in current-based fault detection will become more serious when detecting Type 2 faults; because these faults do not have a characteristic frequency. To effectively detect this type of fault in WTGs, an appropriate time-domain or time-frequency-domain method is required. In this project, a wavelet-filter-based method [11] has been developed for detection of wind turbine Type 2 faults. The proposed wavelet filter is based on discrete wavelet transform (DWT) [14] and wavelet shrinkage [15]. The wavelet filter decomposes the WTG current signal by using the DWT. The fault-related components in the current signal are located in the low energy part of the decomposed sequence due to the subtle and broadband features of these components. A wavelet shrinkage technique is then applied to remove the dominant fault-irrelevant components from the current signal. The low energy points of the decomposed sequence are then identified and added together as the signature of the fault.

In addition, an adaptive noise cancellation method has also been developed as an alternative to the wavelet-filter method for detection of wind turbine Type 2 faults. However, it was found that the wavelet-filter method is superior to the noise cancellation method for detection of Type 2 faults in terms of complexity, implementation, and reliability. Therefore, the adaptive noise cancellation method will not be discussed in this report.

Provided that the fault signature is obtained, a crucial issue is how to quantitatively evaluate the wind turbine condition to determine when maintenance is required. In practical applications, it is desired to evaluate the wind turbine condition solely based on the fault signature in real time. In this project, an impulse detection method [16] has been developed to detect and quantize the excitations (i.e., impulses) in the 1P-invariant PSD of the current or current demodulated signals generated by faults in a wind turbine. In the proposed method, a 1P-invariant PSD spectrum is normalized locally using a suitable moving window in the frequency domain. A median filter is then designed to generate a threshold, from which the impulses are detected from the locally normalized 1P-invariant PSD spectrum. The impulses detected are then used to evaluate the health condition of the wind turbine.

Fig. 1.1 illustrates the use of the proposed technologies for CMFD of a wind turbine, where signal conditioning refers to frequency and amplitude demodulations of the current signal as well as other signal preprocessing functions, such as filtering. Fault signature extraction includes 1P-invariant PSD calculation for Type 1 faults and a wavelet filter for Type 2 faults; and condition evaluation mainly refers to impulse detection. Fig. 1.2 illustrates the details of the functional modules depicted in Fig. 1.1.

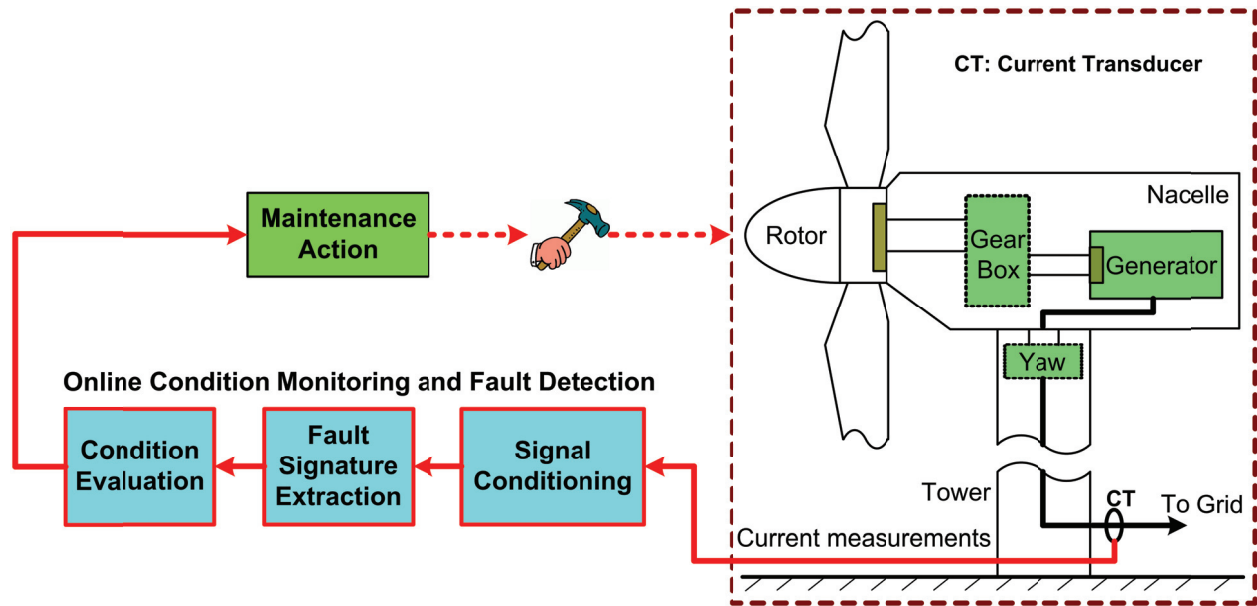


Fig. 1.1: The proposed technologies for CMFD of a wind turbine.

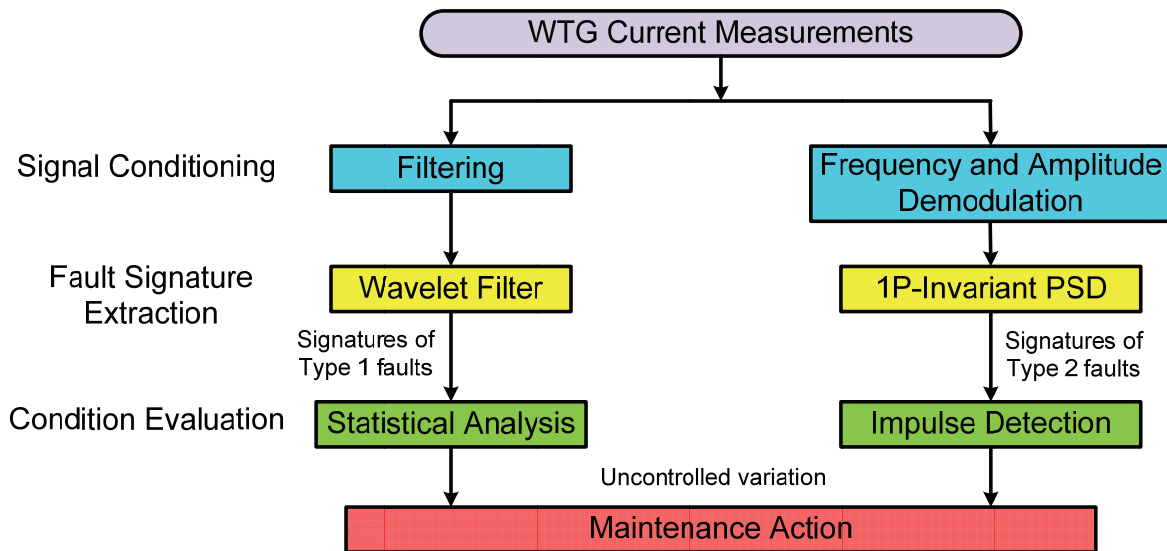


Fig. 1.2: Overall framework of the proposed current-based wind turbine CMFD technologies.

The proposed current-based CMFD technologies provide an effective means to achieve condition-based smart maintenance for wind turbines and have great potential to be adopted by the wind energy industry due to their almost no-cost, nonintrusive features. The outcomes of this project will significantly reduce inspection and maintenance costs, reduce downtime, and improve reliability and the capacity factor of wind turbines. These improvements will make wind energy a reliable, cost-competitive source for clean electricity generation.

## 2. BACKGROUND

### 2.1 Motivation

To produce reliable and cost-effective electric energy from wind, effective maintenance is required to maintain wind turbines in good condition during operation. Effective maintenance can reduce the failure rate and downtime of wind turbines and, consequently, significant losses in electric energy production, reduce the costs associated with repair or replacement of failed components, improve wind turbine capacity factors, and lengthen the life of wind turbines.

Currently, there are hundreds of thousands of wind turbines operating worldwide. This number is expected to continuously increase over the next decade [17], [18]. Most wind turbines are situated on high towers, installed in remote rural areas, distributed over large geographic regions, and subjected to harsh environments and high failure rates. Consequently, O&M of wind turbines requires significant effort and cost. It was reported by [4], [5] that the O&M costs for onshore and offshore wind turbines are in the order of 10-15% and 20-35%, respectively, of the total costs of the generated electricity. Among the total maintenance costs, approximately 25-35% is related to preventive maintenance and 65-75% to corrective maintenance [5]. Currently, in the wind power industry, preventive maintenance is mainly determined by regular inspection and predetermined schedules instead of the actual condition of wind turbines. To make wind energy competitive with traditional forms of energy resources for electricity generation, it is critical to reduce the O&M costs and improve the reliability of wind turbines. Condition-based intelligent maintenance is an effective means to achieve this objective. The benefits of condition-based maintenance include the following:

- Minimize the frequency of inspection and maintenance for wind turbines.
- Prevent unnecessary replacement of components based on time of use.
- Uncover design weakness before failure.
- Detect extreme external conditions to prevent damage of wind turbine components.
- Allow repair rather than replacement of components by detecting fault early.
- Prevent cascading failure and major component failures.
- Minimize wind turbine inspection and maintenance costs, thereby reducing the cost of the electricity generated.
- Increase wind turbine availability and improve the capacity factor; thereby increasing electric energy production.

Most existing technologies for wind turbine CMFD require additional sensors, e.g., vibration sensors, acoustic emission sensors, etc., and data acquisition devices to implement. Most of these sensors are mounted on the surface or buried in the body of wind turbine components, which are difficult to access during wind turbine operation. Measurements that contain the information on wind turbine physical conditions are continuously taken from sensors. These measurements are then evaluated to determine the condition of wind turbines by using appropriate system analysis and signal processing techniques, such as spectrum analysis [19]-[22], wavelet analysis [23]-[25], statistical analysis [26], [27], pattern recognition, envelope curve analysis [28], [29], or neural networks [30]. The use of additional sensors and data acquisition devices increases the cost and hardware complexity of wind turbine systems.

Moreover, the sensors and devices are inevitably subject to failure. According to statistical data reported in [31], sensor failures constitute more than 14% of failures in wind turbines. Sensor failure may further cause the failure of wind turbine control, mechanical, and electrical systems and, consequently, result in significant downtime of the wind turbine. Therefore, the use of additional sensors could cause additional problems with system reliability and additional O&M costs.

On the other hand, some measurements, such as generator currents, are always required for wind turbine control, protection, and grid connection. These measurements are taken by electromagnetic sensing devices, such as current transformers/transducers, which are reliable, robust, and easily accessible from the ground. Therefore, benefit could be achieved by developing new technologies based on current signals, thereby removing the need for additional sensors and data acquisition devices for wind turbine CMFD. The use of current signals can reduce the cost and hardware complexity and improve the reliability of wind turbine systems. Another advantage is that current-based CMFD is nonintrusive and may even be implemented remotely from the wind turbines being monitored. However, little work has been reported on wind turbine CMFD based on current other electrical measurements.

## **2.2 Project Goal and Objectives**

The goal of this project is to develop novel online nonintrusive CMFD technologies for wind turbines. The proposed technologies are based on advanced signal processing and statistical analysis techniques and only use WTG current measurements, which are the same as those used by the wind turbine control and protection system, taken from current transformers/transducers and easily accessible from the ground. Therefore, no additional sensors or data acquisition devices or access to wind turbines is required. Specifically, the following objectives have been achieved in this project:

- Analyze the effects of faults in a WTG on the generator currents of the WTG operating at variable rotating speed conditions from the perspective of amplitude and frequency modulations of the current measurements
- Develop effective amplitude and frequency demodulation methods for appropriate signal conditioning of the current measurements to improve the accuracy and reliability of wind turbine CMFD.
- Develop an effective spectrum analyzer for extracting frequency-domain signatures of faults in wind turbines from generator current measurements.
- Develop an effective wavelet filter for extracting time-frequency-domain signatures of faults in wind turbines from generator current measurements.
- Develop an effective adaptive noise cancellation algorithm for extracting time-domain signatures of faults in wind turbines from generator current measurements.
- Develop an effective statistical fault signature evaluator, which can quantitatively evaluate wind turbine physical conditions and determine when maintenance is required.

- Perform experimental studies on practical small WTGs in the Principal Investigator (PI)'s laboratory to validate the proposed technologies for CMFD in three wind turbine components: bearings, blades, and rotors/shafts.

### **2.3 Qualifications and Experience of the Project Team**

All of the research and development (R&D) activities of this project were performed in the PI's Power & Energy Systems Laboratory at the University of Nebraska-Lincoln (UNL). The laboratory has various state-of-the-art facilities, equipment, and resources, including a wind tunnel, wind turbine simulation platform, various small wind turbines, sensors, and data acquisition systems, etc., to conduct the R&D activities of this project. The PI, Dr. Wei Qiao, has more than seven years of research experience in wind energy systems and more than 15 years of academic and industrial experience in broad areas of power and energy systems. He has published numerous papers in refereed journals and conference proceedings concerning wind energy systems. The project team has extensive R&D experience in various issues, such as control, power electronics, generator design, grid integration, CMFD, etc., of wind energy systems. The project team's R&D projects on wind energy have been supported by a variety of federal, industrial, and other funding sources, including the Department of Energy, National Science Foundation, Department of Transportation, American Public Power Association, Nebraska Center for Energy Sciences Research, Nebraska Public Power District, etc.

### 3. CURRENT-BASED WIND TURBINE CMFD TECHNOLOGIES

#### 3.1 Modulation of Current Signals by a Wind Turbine Fault

Suppose that a wind turbine fault leads to a vibration and, therefore, a shaft torque variation of the WTG at a frequency of  $f_{fault}$ . The WTG current signals are frequency and amplitude modulated by the shaft torque variation at the corresponding characteristic frequency  $f_{fault}$  [7], [8], which is analyzed below.

The shaft torque of a WTG with a fault can be modeled as follows:

$$T(t) = T_0(t) + T_v \cdot \cos(2\pi \cdot f_{fault} \cdot t) \quad (3-1)$$

where  $t$  is the time index,  $T$  is the torque on the wind turbine shaft,  $T_0$  is the torque due to wind power, and  $T_v$  is the amplitude of the shaft torque variation created by the wind turbine fault. The shaft torque variation has a characteristic frequency of  $f_{fault}$ , which is assumed to be constant in steady-state operation of the WTG, where the steady state stands for the slow shaft speed variation due to variable wind power.

If the shaft system of a WTG is simply represented by a one-mass model, the motion equation is given by:

$$J \cdot [d\omega_r(t)/dt] = T(t) - T_e(t) - D \cdot \omega_r(t) \quad (3-2)$$

$$\omega_r(t) = 2\pi \cdot f_r(t) \quad (3-3)$$

where  $J$  is the total inertia constant of the WTG,  $\omega_r$  is the angular shaft rotating speed of the WTG,  $d\omega_r(t)/dt$  is the angular acceleration,  $T_e$  is the electric torque of the WTG,  $D$  is the damping coefficient, which is approximately zero, and  $f_r$  is the shaft rotating frequency or 1P frequency of the WTG.

If the WTG with the fault is operated at steady state, the electric torque  $T_e$  can be expressed by:

$$T_e(t) = T_{e,0}(t) + T_{e,v} \cdot \cos(2\pi \cdot f_{fault} \cdot t + \varphi_e) \quad (3-4)$$

where  $T_{e,0}$  and  $T_{e,v}$  are the electric torques induced by  $T_0$  and  $T_v$ , respectively, and  $\varphi_e$  is the phase shift between the torque variations in the shaft and in the generator created by the wind turbine fault. Therefore, the angular shaft rotating speed is derived from (3-1), (3-2), and (3-4) as follows:

$$d\omega_r(t)/dt = [T_0(t) - T_{e,0}(t)]/J + T_f \cos(2\pi \cdot f_{fault} \cdot t + \varphi_f)/J \quad (3-5)$$

where

$$T_f \cos(2\pi \cdot f_{fault} \cdot t + \varphi_f) = T_v \cdot \cos(2\pi \cdot f_{fault} \cdot t) - T_{e,v} \cdot \cos(2\pi \cdot f_{fault} \cdot t + \varphi_e) \quad (3-6)$$

$$T_f = \{[T_v - T_{e,v} \cdot \cos(\varphi_e)]^2 + [T_{e,v} \cdot \sin(\varphi_e)]^2\}^{1/2} \quad (3-7)$$

$$\varphi_f = \arctan\{[-T_{e,v} \cdot \sin(\varphi_e)]/[T_v - T_{e,v} \cdot \cos(\varphi_e)]\} \quad (3-8)$$

The angular shaft rotating speed can then be calculated by integrating the right-hand side of (3-5):

$$\omega_r(t) = \omega_{r,0} + (1/J) \cdot \int [T_0(t) - T_{e,0}(t)] \cdot dt + (1/J) \cdot \int T_f \cdot \cos(2\pi \cdot f_{fault} \cdot t + \varphi_f) \cdot dt \quad (3-9)$$

Equation (3-9) can be rewritten as:

$$\omega_r(t) = \omega_{r,0} + \omega_{r,w}(t) + \omega_{r,v} \cdot \sin(2\pi \cdot f_{fault} \cdot t + \varphi_f) \quad (3-10)$$

where  $\omega_{r,0}$  is the constant component of the angular shaft rotating speed,  $\omega_{r,w}$  is the angular shaft rotating speed generated by the variable wind power,  $\omega_{r,v}$  is the amplitude of the excitation in the angular shaft rotating speed due to the wind turbine fault. The angular shaft rotating speed,  $\omega_{r,w}$ , and amplitude of excitation in the angular shaft,  $\omega_{r,v}$ , are expressed as follows:

$$\omega_{r,w}(t) = (1/J) \cdot \int [T_0(t) - T_{e,0}(t)] \cdot dt \quad (3-11)$$

$$\omega_{r,v} = 1/(J \cdot 2\pi \cdot f_{fault}) \cdot T_f \quad (3-12)$$

Using (3-3), the shaft rotating frequency of a WTG with a fault can be modeled as:

$$f_r(t) = f_{r,w}(t) + f_{r,v} \cdot \sin(2\pi \cdot f_{fault} \cdot t + \varphi_f) \quad (3-13)$$

where

$$f_{r,w}(t) = [\omega_{r,0} + \omega_{r,w}(t)] / 2\pi \quad (3-14)$$

$$f_{r,v} = \omega_{r,v} / 2\pi \quad (3-15)$$

If the WTG system is equipped with a permanent magnet synchronous generator (PMSG), the relationship between the shaft rotating frequency and the fundamental frequency  $f_1$  of the PMSG stator current signal is:

$$f_1(t) = p \times f_r(t) \quad (3-16)$$

where  $p$  is the number of pole pairs of the PMSG. Using (3-13) and (3-16), the fundamental frequency of the stator current signal is:

$$f_1(t) = p \cdot f_{r,w}(t) + p \cdot f_{r,v} \cdot \sin(2\pi \cdot f_{fault} \cdot t + \varphi_f) \quad (3-17)$$

Therefore, the stator current signal,  $C_s$ , of the PMSG can be modeled as follows:

$$C_s(t) = I_s(t) \cdot \sin\{2\pi \int [p \cdot f_{r,w}(t) + p \cdot f_{r,v} \cdot \sin(2\pi \cdot f_{fault} \cdot t + \varphi_f)] \cdot dt\} \quad (3-18)$$

where the harmonics of the stator current,  $C_s$ , are not considered due to their low magnitudes compared to the fundamental-frequency component; and  $I_s$  is the amplitude of the stator current signal. It shows that the stator current signal of a direct-drive PMSG wind turbine is frequency modulated by the shaft torque variation generated by the wind turbine fault.

The amplitude of the voltage,  $E_s$ , induced in a given stator phase is:

$$E_s(t) = K \cdot \phi \cdot f_1(t) \quad (3-19)$$

where  $K$  is a constant representing the structure of the PMSG;  $\phi$  is the total flux in the PMSG. The amplitude of the phase current  $I_s$  is:

$$I_s(t) = E_s(t) / |Z_s(t)| \quad (3-20)$$

where  $Z_s$  is the equivalent complex impedance of the PMSG stator circuit and the external circuit or load to which the PMSG is connected. According to (3-17), (3-19), and (3-20), the amplitude of the stator current signal,  $I_s$ , can be presented as:

$$I_s(t) = I_{s.w}(t) + I_{s.v}(t) \cdot \sin(2\pi \cdot f_{fault} \cdot t + \varphi_f) \quad (3-21)$$

$$I_{s.w}(t) = K \cdot \phi \cdot p \cdot f_{r.w}(t) / |Z_s(t)| \quad (3-22)$$

$$I_{s.v}(t) = K \cdot \phi \cdot p \cdot f_{r.v} / |Z_s(t)| \quad (3-23)$$

It shows that the stator current signal of the PMSG is also amplitude modulated by the shaft torque variation created by the wind turbine fault.

If the WTG system is equipped with a doubly fed induction generator (DFIG), the relationship between the shaft rotating frequency and the electrical frequency  $f_{rotor}$  of the DFIG rotor current signal is given below:

$$f_{rotor}(t) = p \times f_r(t) - f_{syn} \quad (3-24)$$

where  $p$  is the number of pole pairs of the DFIG, and  $f_{syn}$  is the frequency of the DFIG stator current, which is normally constant at 50 or 60 Hz. Using (3-13) and (3-24), the electrical frequency of the rotor current signal is:

$$f_{rotor}(t) = p \cdot f_{r.w}(t) + p \cdot f_{r.v} \cdot \sin(2\pi \cdot f_{fault} \cdot t + \varphi_f) - f_{syn} \quad (3-25)$$

Therefore, the rotor current signal,  $C_r$ , of the DFIG can be modeled as follows:

$$C_r(t) = I_r(t) \cdot \sin\{2\pi \int [p \cdot f_{r.w}(t) + p \cdot f_{r.v} \cdot \sin(2\pi \cdot f_{fault} \cdot t + \varphi_f) - f_{syn}] \cdot dt\} \quad (3-26)$$

where  $I_r$  is the amplitude of the rotor current signal. It shows that the rotor current signal of a DFIG wind turbine is frequency modulated by the shaft torque variation generated by the wind turbine fault.

The amplitude of the induced rotor voltage,  $E_r$ , in a DFIG is:

$$E_r(t) = -s \cdot E_{r0} \quad (3-27)$$

$$s = -f_{rotor}(t) / f_{syn} \quad (3-28)$$

where  $s$  is the slip of the DFIG, and  $E_{r0}$  is the magnitude of the induced rotor voltage at locked-rotor conditions, which is a constant at a given grid voltage level. The amplitude of the DFIG rotor current,  $I_r$ , is:

$$I_r(t) = E_r(t) / |Z_r(t)| \quad (3-29)$$

where  $Z_r$  is the equivalent complex impedance of the DFIG rotor circuit and the external circuit to which the DFIG rotor windings are connected. According to (3-24), (3-27), (3-28), and (3-29), the amplitude of the rotor current signal,  $I_r$ , can be presented as:

$$I_r(t) = I_{r.w}(t) + I_{r.v}(t) \cdot \sin(2\pi \cdot f_{fault} \cdot t + \varphi_f) \quad (3-30)$$

$$I_{r.w}(t) = E_{r0} \cdot [p \cdot f_{r.w}(t) - f_{syn}] / [|Z_r(t)| \cdot f_{syn}] \quad (3-31)$$

$$I_{r.v}(t) = E_{r0} \cdot p \cdot f_{r.v} / [|Z_r(t)| \cdot f_{syn}] \quad (3-32)$$

It shows that the rotor current signal of the DFIG is also amplitude modulated by the shaft torque variation created by the wind turbine fault.

### 3.2 Current Demodulation

The WTG current signals are frequency and amplitude modulated by the vibration generated by a wind turbine fault [7], [8]. According to (3-18), (3-21), (3-26), and (3-30), the stator current,  $C_s$ , of a PMSG and the rotor current,  $C_r$ , of a DFIG are:

$$C_s(t) = I_s(t) \cdot \sin\left[2\pi \int p \cdot f_r(t) \cdot dt\right] \quad (3-33)$$

$$C_r(t) = I_r(t) \cdot \sin\left\{2\pi \int [p \cdot f_r(t) - f_{syn}] \cdot dt\right\} \quad (3-34)$$

Therefore, not only frequency demodulation methods can be used to discover the excitations in  $f_r(t)$  related to a wind turbine fault, but also amplitude demodulation methods can be applied to extract the vibrations in  $I_s(t)$  or  $I_r(t)$  created by the wind turbine fault. To improve the accuracy of fault detection and increase the redundancy and reliability of the fault detection system, both the frequency and amplitude demodulation methods can be applied.

#### 3.2.1 Frequency Demodulation

In a WTG, the shaft rotating frequency information is normally required for maximum power point tracking control. The shaft rotating frequency is usually measured by using a position/speed sensor, e.g., an encoder or resolver, or can be estimated from the WTG current measurements using an observer. The shaft rotating frequency is the frequency demodulated signal of current and can be used for WTG fault detection. A simple method (i.e., observer) to demodulate the frequency from a stator current signal of a PMSG is the PLL method [32], as shown in Fig. 3.1, where the frequency of the input signal is calculated by using a voltage controlled oscillator. The input signal is the measured stator current,  $C_s$ , of a PMSG or the rotor current,  $C_r$ , of a DFIG. By using the PLL method,  $C_s$  or  $C_r$  is frequency demodulated to obtain the PMSG stator current fundamental frequency,  $f_{1,e}$ , or DFIG rotor current frequency,  $f_{rotor,e}$ , respectively, given as:

$$f_{1,e}(t) = p \cdot f_{r,w}(t) + p \cdot f_{r,v} \cdot \sin(2\pi \cdot f_{fault} \cdot t + \varphi_f) + e_1(t) \quad (3-35)$$

$$f_{rotor,e}(t) = p \cdot f_{r,w}(t) + p \cdot f_{r,v} \cdot \sin(2\pi \cdot f_{fault} \cdot t + \varphi_f) - f_{syn} + e_r(t) \quad (3-36)$$

where  $e_1(t)$  and  $e_r(t)$  are the errors between the real and estimated stator current fundamental frequencies. The values of  $e_1(t)$  and  $e_r(t)$  are almost zero and can be neglected.

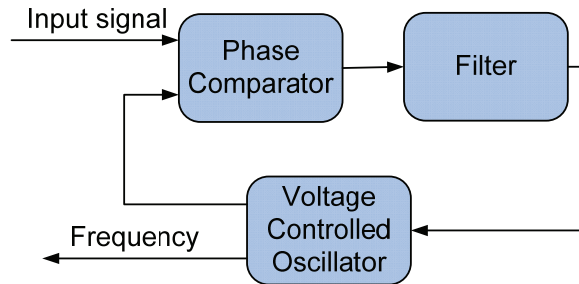


Fig. 3.1: Schematic diagram of a PLL for signal frequency demodulation.

### 3.2.2 Amplitude Demodulation

Moreover, an amplitude demodulation method can be applied to calculate the variable amplitudes  $I_s(t)$  or  $I_r(t)$  of current measurements in (3-33) and (3-34), respectively. For instance, the square law, which is a classical method for amplitude demodulation or envelope detection, can be used to extract the variable amplitudes of a current signal.

According to (3-21), the current signal of a PMSG wind turbine in (3-33) can be rewritten as:

$$C_s(t) = [I_{s,w}(t) + I_{s,v}(t) \cdot \sin(2\pi \cdot f_{fault} \cdot t + \varphi_f)] \cdot \sin[\theta(t)] \quad (3-37)$$

$$\theta(t) = 2\pi \cdot \int p \cdot f_r(t) \cdot dt \quad (3-38)$$

Apply the square law to the signal,  $C_s$ :

$$C_s(t)^2 = \{[I_{s,w}(t) + I_{s,v}(t) \cdot \sin(2\pi \cdot f_{fault} \cdot t + \varphi_f)] \cdot \sin[\theta(t)]\}^2 \quad (3-39)$$

Rewrite (3-39) by using trigonometric functions and sort the components from low frequency to high frequency:

$$\begin{aligned} C_s(t)^2 = & [I_{s,w}^2(t)/2 + I_{s,v}^2(t)/4] + I_{s,w}(t) \cdot I_{s,v}(t) \cdot \sin(2\pi \cdot f_{fault}(t) \cdot t + \varphi_f) - I_{s,v}^2(t) \cdot \cos[4\pi \cdot f_{fault}(t) \cdot t + 2\varphi_f]/4 + \\ & I_{s,v}^2(t) \cdot \cos[2\theta(t) - 4\pi \cdot f_{fault} \cdot t - 2\varphi_f]/8 + I_{s,w}(t) \cdot I_{s,v}(t) \cdot \cos[2\theta(t) - 2\pi \cdot f_{fault} \cdot t - \varphi_f]/2 - \\ & [I_{s,w}^2(t)/2 + I_{s,v}^2(t)/4] \cdot \cos[2\theta(t)] - I_{s,w}(t) \cdot I_{s,v}(t) \cdot \cos[2\theta(t) + 2\pi \cdot f_{fault} \cdot t + \varphi_f]/2 + \\ & I_{s,v}^2(t) \cdot \cos[2\theta(t) + 4\pi \cdot f_{fault} \cdot t + 2\varphi_f]/8 \end{aligned} \quad (3-40)$$

where the current squared signal,  $C_s^2$ , is the amplitude demodulated signal of the current,  $C_s$ ; “ $I_{s,w}(t) \cdot I_{s,v}(t) \cdot \sin(2\pi \cdot f_{fault}(t) \cdot t + \varphi_f)$ ” is an excitation due to the WTG fault; and “ $I_{s,v}^2(t) \cdot \cos[4\pi \cdot f_{fault}(t) \cdot t + 2\varphi_f]/4$ ” is the second harmonic of the excitation in  $C_s^2$  generated by the WTG fault. Both terms can be used for fault detection. Since the fundamental frequency is the dominant component in the stator current signal, the magnitude of  $I_{s,w}(t)$  is much larger than that of  $I_{s,v}(t)$ . Therefore, the second harmonic of the excitation generated by the WTG fault has a low magnitude and can be neglected.

### 3.2.3 Benefits of Using Current Demodulation

Using the demodulated signals for WTG fault detection has obvious advantages over directly using the stator current measurements. The major noise in WTG current signals and current demodulated signals are the fundamental-frequency component and the DC component, respectively. The DC component can be easily removed compared to the fundamental-frequency component. Furthermore, if stator current measurements are directly used for WTG fault detection, the energy of excitations related to WTG faults will disperse to multiple characteristic frequencies. The magnitudes of excitations at these multiple characteristic frequencies are then less outstanding than those at the only fault characteristic frequency,  $f_{fault}$ , of the current demodulated signals in the frequency domain.

## 3.3 1P-Invariant PSD Method

Since the fault characteristic frequencies of a WTG vary with the shaft rotating frequency during variable-speed operating condition of the WTG, it is difficult to extract the fault signatures from

the nonstationary current signals of the WTG using classical frequency spectrum analysis methods. However, if a WTG rotates at a constant frequency, the classical frequency spectrum analysis could be used to identify a WTG fault effectively based on its characteristic frequencies. Therefore, if the WTG current signals or current demodulated signals are preprocessed in such a way that the variable fault characteristic frequencies of the WTG are converted to constant values, the classical frequency spectrum analysis methods, e.g., PSD, can then be used to detect the faults for a variable-speed WTG.

Define  $\Omega_r$  as the normalized frequency of a current demodulated signal; and define  $f_s$  as the sampling frequency of the current measurements. The relationship among  $f_r$  (shaft rotating frequency),  $f_s$ , and  $\Omega_r$  can be written as:

$$\Omega_r(t) / 2\pi = f_r(t) / f_s \quad (3-41)$$

where  $\Omega_r(t)$  is expected to be constant to facilitate the fault detection by using classical frequency spectrum analysis. Therefore, if the sampling frequency,  $f_s$ , is changed continuously with  $f_r(t)$  to make the right-hand side of (3-41) constant,  $\Omega_r(t)$  will become constant. The proposed method preprocesses the current demodulated signal of a WTG to obtain a constant  $\Omega_r(t)$ , which is shown in Fig. 3.2 and implemented in the following steps [8], [9].

- (1) Choose an up-sampling ratio,  $M$ , and a base value of the down-sampling step size  $L$ .
- (2) Sample the measured nonstationary current  $i(t)$  of the WTG with a fixed sampling rate; the result is  $c(n)$ , where  $n = 1, 2, 3, \dots, N$  and  $N$  is the length of the current measurement.
- (3) Demodulate the frequency and amplitude of the nonstationary current signal  $c(n)$ ; the results are a current frequency demodulated signal  $s_f(n)$  and a current amplitude demodulated signal  $s_a(n)$ .
- (4) Estimate the shaft rotating frequency,  $f_r(n)$ , by using the current frequency demodulated signal,  $s_f(n)$ ; and choose a base frequency,  $f_b$ , based on  $f_r(n)$ . For a PMSG,  $f_r(n) = s_f(n)/p$ ; for a DFIG,  $f_r(n) = [s_f(n) + f_{syn}]/p$ .
- (5) Up-sample (interpolate)  $f_r(n)$ ,  $s_f(n)$ , and  $s_a(n)$  by a constant up-sampling ratio of  $M$ ; the results are  $f_{r,up}(k)$ ,  $s_{f,up}(k)$ , and  $s_{a,up}(k)$ , respectively, where  $k = 1, 2, 3, \dots, M \times N$ .
- (6) Down-sample  $s_{f,up}(k)$  and  $s_{a,up}(k)$  by a variable down-sampling step size; the results are  $s_{f,down}(j)$  and  $s_{a,down}(j)$ , respectively, where  $j = 1, 2, 3, \dots, J$  and  $J$  is determined by  $M$ ,  $N$ , and  $L$ . Suppose that  $s(n)$  stands for  $s_f(n)$  or  $s_a(n)$ ;  $s_{down}(j)$  stands for  $s_{f,down}(j)$  or  $s_{a,down}(j)$ ; and  $s_{up}(k)$  stands for  $s_{f,up}(k)$  or  $s_{a,up}(k)$ . In the down-sampling process:

$$s_{down}(1) = s_{up}(1) \quad (3-42)$$

If  $s_{down}(j) = s_{up}(k)$ , then,

$$s_{down}(j+1) = s_{up}(k + \text{round}[L \cdot f_b / f_{r,up}(k)]) \quad (3-43)$$

where  $\text{round}[L \cdot f_b / f_{r,up}(k)]$  is the variable down-sampling step size, which depends on the up-sampled shaft rotating frequency,  $f_{r,up}(k)$ ; and  $\text{round}(\cdot)$  stands for rounding a number to the nearest integer. The down-sampling process to obtain  $s_{down}(j)$  is equivalent to resampling the original or up-sampled current demodulated signal [ $s(n)$  or  $s_{up}(k)$ , respectively] with a variable sampling frequency,  $f_s(k)$ , whose value is proportional to the value of  $f_{r,up}(k)$ . According to (3-41), the normalized frequency of

$s_{down}(j)$ , which is  $\Omega_{down}(j)$ , is given by:

$$\Omega_{down}(j) / 2\pi = s_{down}(j) / f_s(j) \quad (3-44)$$

where  $\Omega_{down}(j)$  is now a constant value.

- (7) Calculate the classical frequency spectrum, e.g., PSD, of the down-sampled current demodulated signal  $s_{down}(j)$  for the fault signature extraction, which now has a constant characteristic frequency.

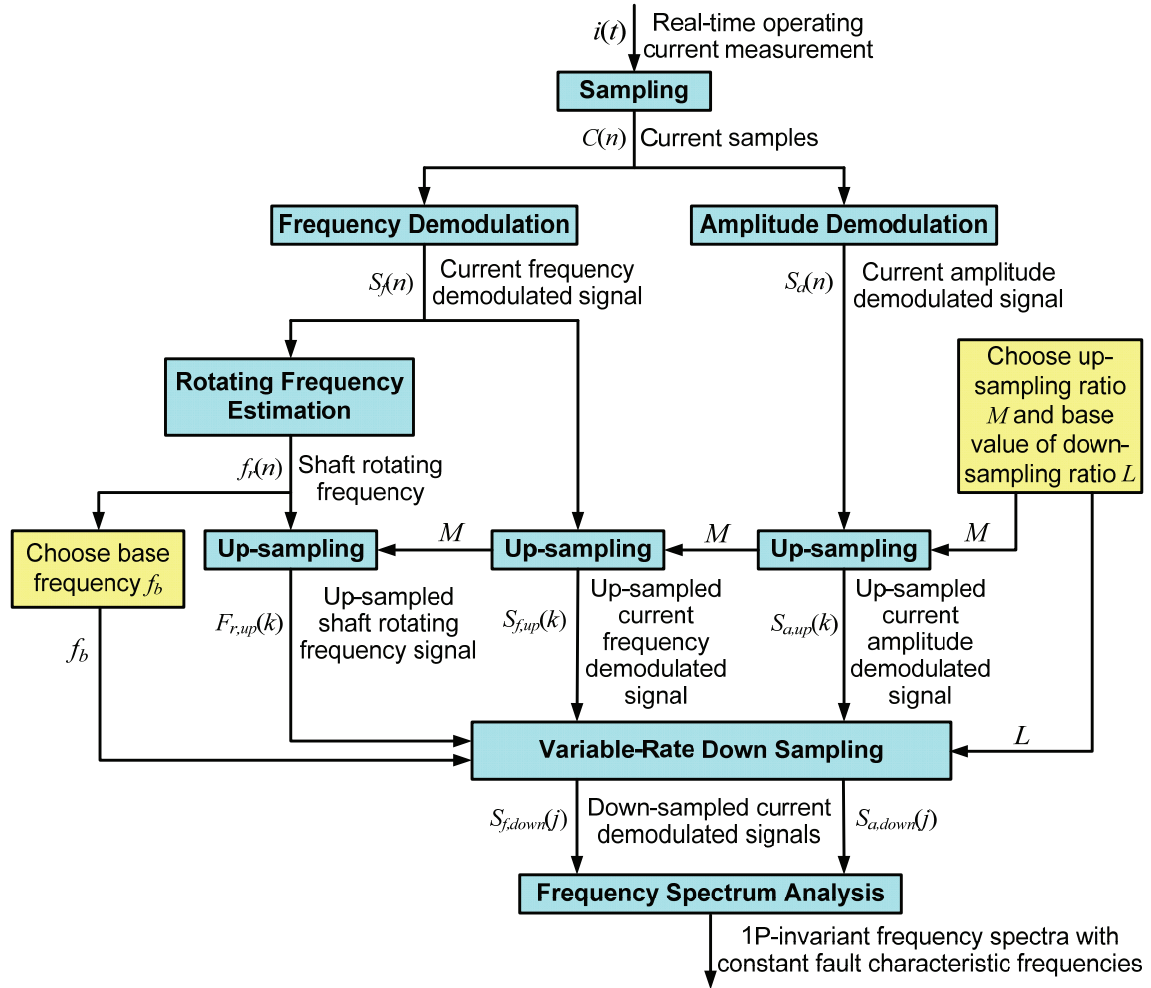


Fig. 3.2: Schematic diagram of the 1P-invariant PSD method.

By using the proposed method, the variable characteristic frequency,  $f_{fault}$ , of a WTG fault becomes a constant value in the frequency spectrum of  $s_{down}(j)$ . Therefore, the resulting PSD spectrum is called the 1P-invariant PSD spectrum; and the magnitude of the excitation at  $f_{fault}$  in the PSD spectrum of  $s_{down}(j)$  can be used as a signature to clearly identify and quantify the WTG fault. In the proposed method, the constant base value of the down-sampling step size,  $L$ , should be chosen based on two criteria. First,  $L$  should be large enough to eliminate the quantization error due to the requirement of an integral down-sampling step size. Second,  $L$  should be small

enough to ensure that the sampling frequency after down sampling is greater than twice the  $f_{fault}$  frequency. Normally,  $L$  should be larger than 10. The base frequency,  $f_b$ , is chosen to be the mean value of the estimated shaft rotating frequency,  $f_r(n)$ . Furthermore, if the measured current is sampled with a sufficiently high sampling rate in Step (2) such that the sampling frequency of the down-sampled signal,  $s_{down}(j)$ , without using up-sampling, is greater than twice the characteristic frequency of the WTG fault, then  $M$  is 1 and Step (5) is not necessary.

### 3.4 Wavelet Filter

Since the Type 2 faults do not have characteristic frequencies, traditional frequency-domain analysis-based methods are not effective in detecting these faults. In this project, a wavelet-filter-based method [11] has been developed for detection of Type 2 faults in a WTG, as shown in Fig. 3.3. The proposed wavelet filter is based on the wavelet transform and wavelet shrinkage techniques. The wavelet transform decomposes the original raw current signal into two parts: trend subsignals and fluctuations. High energy components of the raw current signal, which are the dominant noise components irrelevant to the fault, are compacted to its trend subsignals, while the fluctuations only contain the weak-energy components which are mainly the fault-related components. This process is called compaction of energy, which is one of the main characteristics of wavelet transform. Here energy is defined as the square of the signal. The wavelet shrinkage technique is then applied to work in a way similar to an adaptive notch filter to remove the fault-irrelevant dominant components from the raw current signal. The remaining components are weak-energy components mainly related to the fault. The ratio between the total energy of the weak-energy components and the total energy of the raw signal is then used as a fault signature. As the physical condition of a wind turbine component becomes worse and worse, the magnitude of the energy of the fault-related components becomes more and more significant, which results in the increase of the fault signature.

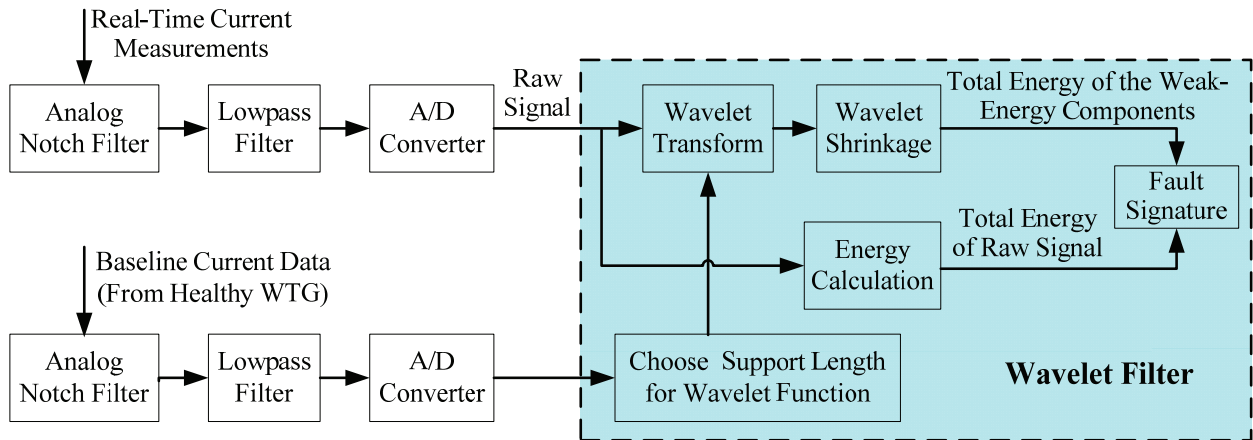


Fig. 3.3: Schematic diagram of the wavelet filter method.

Note that in the wavelet filter method, the current signal, instead of the current demodulated signal, is used. The notch filters are used to remove the fundamental-frequency component of

the current signal. The lowpass filters are used for antialiasing. The baseline current data are the first several samples obtained from the healthy WTG, as it is assumed that the WTG is healthy initially. These baseline current data are used to determine the support length of the wavelet function.

### 3.5 Impulse Detection

An impulse detection method [16] has been developed for automatic extraction of fault signatures from the 1P-invariant PSD spectra. The 1P-invariant PSD spectra of the current demodulated signals usually have nonstationary amplitudes. Therefore, a localized method is required for impulse detection from the PSD spectra. In a 1P-invariant PSD spectrum, the magnitude at one frequency represents the energy of the time-domain signal at that frequency. If the energy around a certain frequency is high, it will generate an impulse in the PSD spectrum. The impulse detection method is proposed based on the amplitude of a 1P-invariant PSD spectrum.

Assume that  $x(f)$  is the sampled 1P-invariant PSD spectrum of a current demodulated signal, where  $f=1, 2, 3, \dots, F$  and  $F$  is the length of  $x(f)$ . Define the energy of the current demodulated signal at the frequency,  $f$ , as:

$$P_x(f) = x(f) \quad (3-45)$$

If a moving window of length  $2W+1$  is applied to  $x(f)$ , the energy of the signal in the window is defined as:

$$P_w(f) = x(f-W) + x(f-W+1) + \dots + x(f+W) \quad (3-46)$$

The ratio  $R(f)$  is defined to present the percentage of the energy of the current demodulated signal at the frequency,  $f$ , with respect to the total energy of the signal at all of the frequencies contained in the moving window:

$$R(f) = P_x(f) / P_w(f) \quad (3-47)$$

The resulting  $R(f)$  represents the locally normalized 1P-invariant PSD of the current demodulated signal. If  $R(f)$  at a certain frequency point is greater than a threshold,  $T$ , it indicates that there is an impulse at that frequency. In practice, it is important to automatically generate the threshold,  $T$ , from the PSD spectrum. The median filter, which is a nonlinear filter, is well known for impulse removal [33]. Define  $R_f(f)$  the result of  $R(f)$  processed by a median filter. The threshold,  $T$ , is then set to be the maximum value of  $R_f(f)$ . Since the impulses that are not generated by the WTG faults have been removed from the 1P-invariant PSD spectrum of the current demodulated signal during a pretreatment process, the impulses generated by the WTG faults have the highest amplitudes in the 1P-invariant PSD spectrum of the current demodulated signal. In this work, a three-order median filter is chosen to calculate  $R_f(f)$  and the threshold,  $T$ . The  $R_f(f)$  is calculated by:

$$R_f(f) = \text{Median}[R(f-1), R(f), R(f+1)] \quad (3-48)$$

where  $\text{Median}[X]$  stands for selecting the median of the data set  $X$ . The threshold,  $T$ , is then obtained as:

$$T = \text{Maximum}[R(f)] \quad (3-49)$$

where  $\text{Maximum}[\ ]$  stands for the maximum value of  $R(f)$ .

In the 1P-invariant PSD, the amplitudes of the impulses at the characteristic frequencies of WTG faults are the signature for wind turbine fault detection. Since there are no impulses at the characteristic frequencies of faults when the WTG is healthy, an alarm will be generated if an impulse is detected at a characteristic frequency of WTG faults.

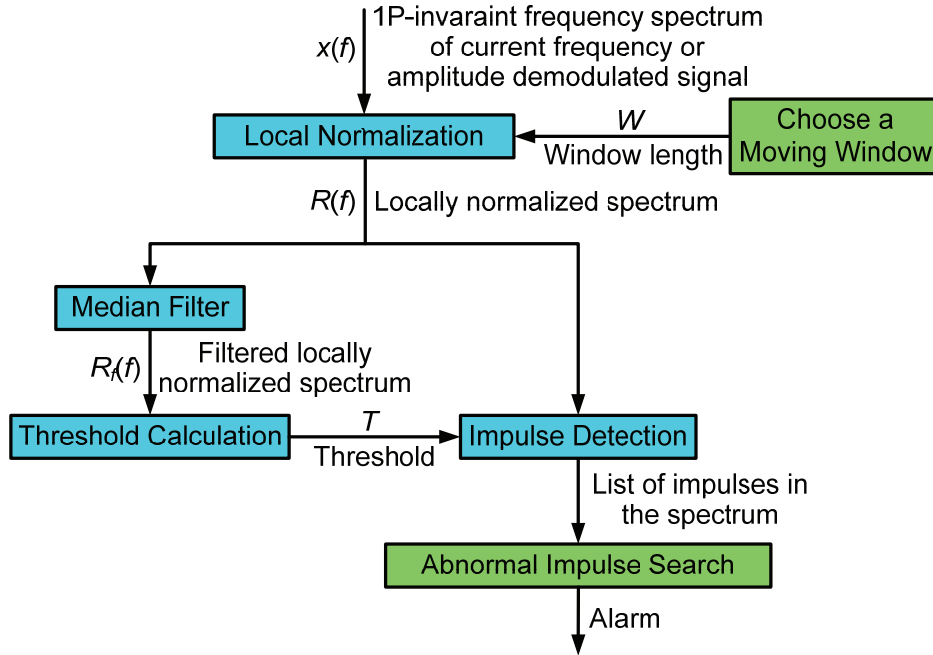


Fig. 3.4: Schematic diagram of the impulse detection method.

## 4. SIMULATION AND EXPERIMENTAL VALIDATION PLATFORMS

Extensive simulation and experimental studies have been performed in the PI's laboratory to validate the proposed technologies for CMFD of small direct-drive PMSG wind turbines in three wind turbine components: bearings, blades, and rotors/shafts. This section describes the simulation and experimental platforms used to validate the proposed current-based online wind turbine CMFD technologies.

### 4.1 Simulation Validation Platform

The simulation validation platform includes the dynamical model of a 10-kW direct-drive WTG developed in a combined environment of FAST (Fatigue, Aerodynamics, Structures, and Turbulence) [34], TurbSim [35], and Simulink, as illustrated in Fig. 4.1, where TurbSim generates the wind data; FAST simulates the dynamics of the wind turbine; and Simulink simulates the dynamics of the generator and other electrical components of the WTG system.

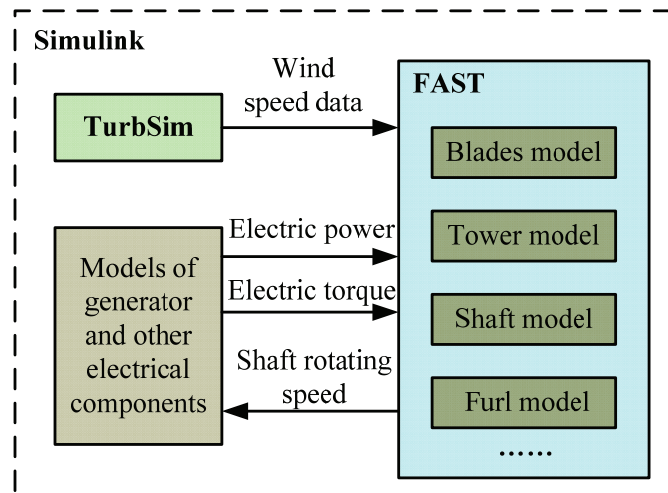


Fig. 4.1: Structure of the simulation validation platform.

#### 4.1.1 WTG Model

FAST version 7.0 was used to simulate the dynamics of the wind turbine. FAST is an aeroelastic code developed initially by Oregon State University. It is one of the most advanced design codes for horizontal-axis wind turbines. In the simulation study, FAST works as a subroutine in Simulink. The signals of the electric power, electric torque, and shaft rotating speed are used to connect the FAST and Simulink models of the WTG system. The model wind turbine in FAST mainly includes tower, blades, shaft, furl, and support platform. The hub height of the wind turbine is 34 meters. The wind turbine has 3 blades with a rotor diameter of 2.9 meters and an upwind configuration. A 48-pole PMSG was simulated in Simulink to convert mechanical energy from the turbine into electric energy. One phase stator current signal of the PMSG was

recorded for wind turbine fault detection.

#### 4.1.2 Wind Speed Data

TurbSim, which is a stochastic, full-field, turbulent wind simulator developed by the National Renewable Energy Laboratory (NREL) [35], was used in the simulation study to produce wind velocity vectors in a time series across the entire rotating plane of the wind turbine's rotor. An average wind speed of 12 m/s was chosen in the simulation study. The IEC Kaimal turbulence model was used to generate wind turbulence in all simulations. The cross-section area (8m×8m) of the wind flow was divided into a 6×6 grid where the wind velocity and direction were calculated by TurbSim for each grid cell. The output of TurbSim contains a time series of wind speed, which was used for the aeroelastic simulation in FAST.

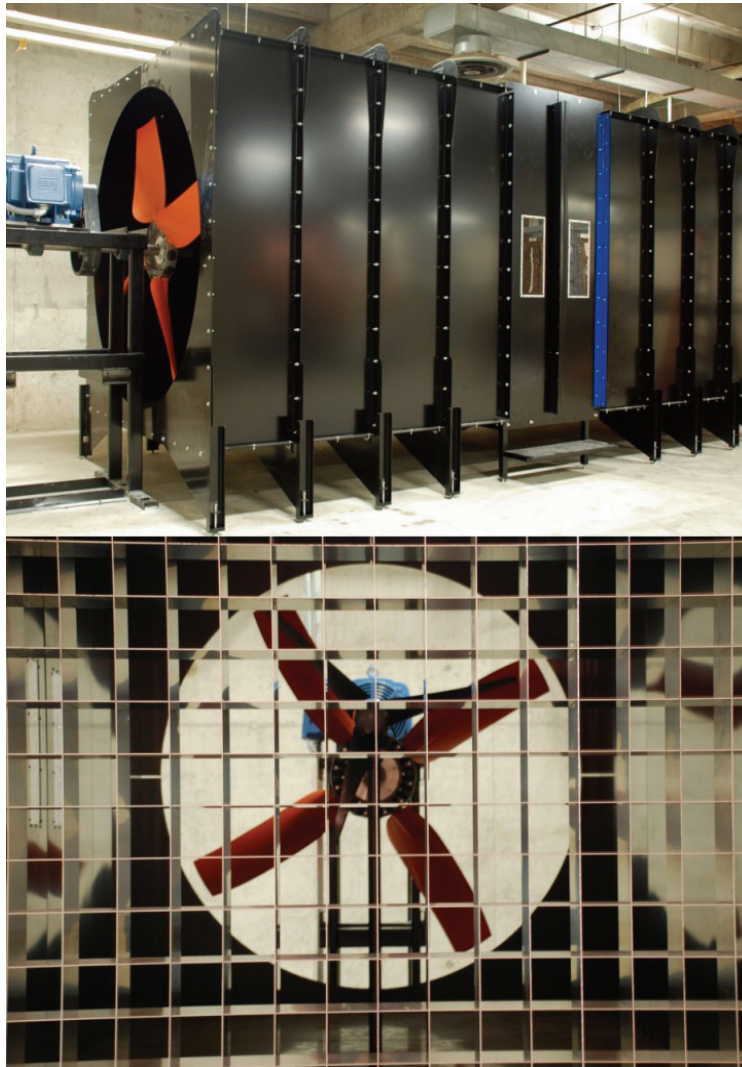


Fig. 4.2: The wind tunnel with a testing WTG in the UNL's Power & Energy Systems laboratory.

## 4.2 Experimental Validation Platform

The WTGs used for experimental studies are small direct-drive PMSG wind turbines. They were tested in a wind tunnel with the dimensions of 2.5 meter  $\times$  2.5 meter  $\times$  6.5 meter in the UNL's Power & Energy Systems Laboratory, as shown in Fig. 4.2. The wind tunnel uses a variable-speed fan to generate controllable wind flows with the speed from 0 to 10 m/s. In the experiments, the rotating speed of the fan was varied to generate variable wind speed in the wind tunnel. Consequently, the WTGs were operated in variable-speed conditions.

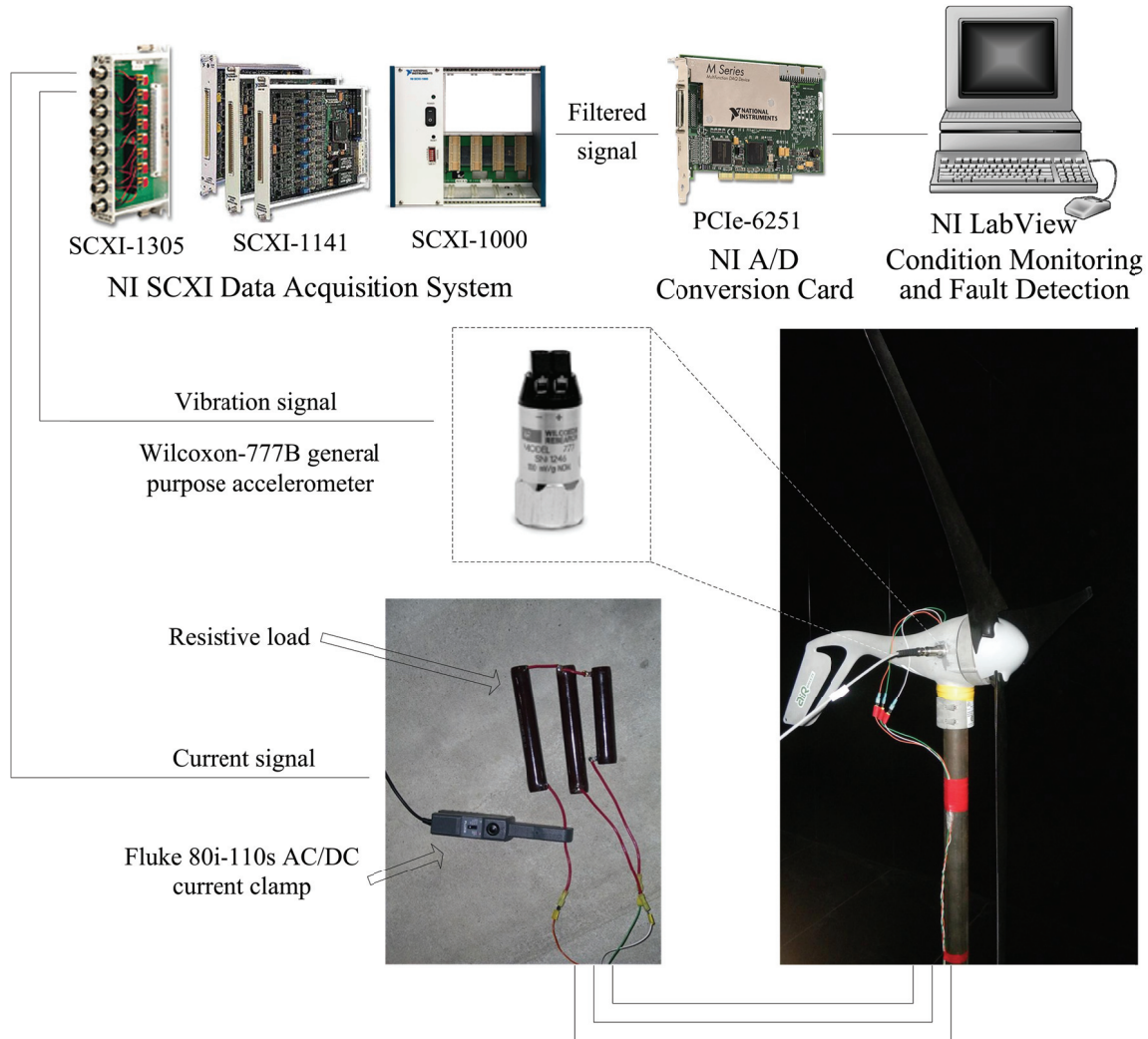


Fig. 4.3: Sensing and data acquisition system for the testing WTGs.

Fig. 4.3 shows the sensing and data acquisition system used for the testing WTGs in the experiments. One phase stator current of the WTGs was recorded via a Fluke 80i-110s AC/DC current clamp. A general purpose accelerometer (Wilcoxon-777B) was mounted on the testing WTGs to measure its vibration. Due to a larger stiffness in the vertical direction and a smaller

stiffness in the horizontal direction of the tower of the WTG [36], the amplitude of vibration in the horizontal direction is much greater than that in the vertical direction. Therefore, the accelerometer was mounted on the surface of the nacelle to detect the vibration in the horizontal direction of the wind turbine. The measured vibration and current signals were digitalized by a National Instrument data acquisition system, where the SCXI-1141 card was used as an antialiasing filter; the PCIe-6251 card is an A/D converter; the SCXI-1305 and SCXI-1000 are the interface and enclosure of the data acquisition system, respectively. The sampling rate was 10 kHz. The current and vibration samples were acquired by the LabView software operating on a lab computer. These samples were then used for CMFD of the testing WTGs using the proposed technologies.

## 5. WIND TURBINE IMBALANCE FAULT DETECTION

Imbalance faults constitute a significant portion of all faults in WTGs [37]. A common imbalance fault in WTGs is shaft/blade imbalance. A blade imbalance can be caused by errors in manufacturing and construction, icing, deformation due to aging, or wear and fatigue during the operation of the WTG. Components tend to shift and wear in varying degrees over time, causing imbalance on the rotating shaft/blades. Another common imbalance fault is aerodynamic asymmetry, which can be caused by several factors, including high wind shear and errors in the control mechanism. If the pitch of one blade is slightly different from the other two blades due to errors in the control mechanism, the torque on the rotating shaft will not be balanced, leading to aerodynamic asymmetry. A small imbalance fault can cause significant consequences on the towers and the WTGs. For instance, a blade imbalance caused by icing can create additional loads on the supporting tower of the wind turbine, which may lead to fractures and possible collapses [38] of the tower. Due to WTGs' delicate structure and high repairing cost [3], [37], [39], effective imbalance fault detection is of significant interest to the wind power industry.

### 5.1 The Characteristic Frequencies of Imbalance Faults

It has been reported that the spectra of the shaft torque and the output electric power of a WTG with three blades are determined by certain events. The vibration at 3P frequency, which is three times the shaft rotating frequency of a WTG, is generated by the effect of yaw error, wind shear, or tower shadow [12], [40]. The vibration at 1P frequency is created by imbalance faults, including blade imbalance and aerodynamic asymmetry [9], [13], [19], [41]. Moreover, these events also affect the shaft rotating frequency of the WTG and produce excitations at the corresponding frequencies in the shaft rotating frequency signals.

When an imbalance fault occurs on the shaft of a WTG, an additional force will be induced in the shaft. In the case of blade imbalance where the mass distribution of one blade is different from others, a rotor mass imbalance will occur and induce vibrations in the shaft rotating speed of the WTG. This is illustrated in Fig. 5.1, where  $m_R$  is the equivalent imbalance mass;  $r_R$  is the distance between the equivalent imbalance mass and the center of the shaft; and  $\omega_r$  is the angular shaft rotating speed. When the equivalent imbalance mass rotates from the top to the bottom of the rotating plane, the power of gravity accelerates the shaft. On the other hand, when the equivalent imbalance mass rotates from the bottom to the top of the rotating plane, the power of gravity decelerates the shaft. Consequently, the shaft rotating speed vibrates at the frequency of 1P.

Aerodynamic asymmetry stands for that the force affected on one blade is different from those on other blades. Aerodynamic asymmetry along with yaw error, wind shear, or tower shadow together influences the shaft rotating speed of a WTG. For example, Fig. 5.2 shows the effect of an aerodynamic asymmetry caused by wind shear, where  $F_{wind}$  is the force of the wind flow affected on the blades;  $F_t$  is the force of the wind flow affected on the blade that is on the top of the rotating plane;  $F_b$  is the force of the wind flow affected on the blade that is on the bottom of the rotating plane. The amplitude of  $F_t$  is always greater than that of  $F_b$  due to the effect of wind shear, which follows the following power law.

$$U(z)/U(z_r) = (z/z_r)^\alpha \quad (5-1)$$

where  $U(z)$  and  $U(z_r)$  are wind velocities at height  $z$  and the reference height  $z_r$ , respectively; and  $\alpha$  is the power law exponent [42].

Normally, a blade has the largest acceleration caused by  $F_t$  and the smallest acceleration caused by  $F_b$ . Therefore, a vibration at the 3P frequency is produced in the shaft speed by wind shear in a balanced wind turbine with three blades. In the case of an aerodynamic asymmetry, a blade of the turbine has different  $F_t$  and  $F_b$  from the other two blades. As a result, the acceleration and deceleration of the imbalanced blade produce a vibration at the 1P frequency in the shaft speed. On the other hand, the other two blades have different  $F_t$  and  $F_b$  from the imbalanced one. As a result, a vibration also appears at the 2P frequency in the shaft speed signal.

The characteristic frequencies of shaft/blade imbalance and aerodynamic asymmetry both appear at the 1P frequency in the shaft speed signal of a wind turbine. Therefore, the excitations of the shaft speed signal at the 1P frequency can be used as a signature for imbalance fault detection.

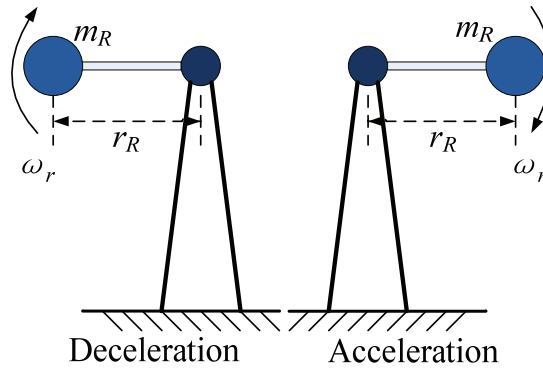


Fig. 5.1: Effect of blade imbalance of a wind turbine.

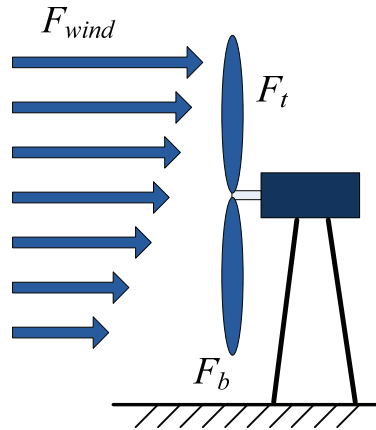


Fig. 5.2: Effect of an aerodynamic asymmetry of a wind turbine caused by wind shear.

## 5.2 Simulation Study of Imbalance Fault Detection

Simulations were performed for the 10-kW model WTG described in Section 4.1 in the healthy condition (i.e., the baseline case) as well as in two imbalance fault conditions: blade imbalance and aerodynamic asymmetry [9]. The blade imbalance was simulated by changing the mass density of one blade, which created an uneven distribution of mass with respect to the rotor. The aerodynamic asymmetry was simulated by adjusting the pitch of one blade, which created an uneven torque across the rotor. One phase stator current of the WTG was recorded in the simulations to estimate the shaft rotating frequency. The proposed method was then applied to extract the signatures of the faults from the recorded data in the frequency domain.

The mass density of one blade was scaled up and down in the simulations of blade imbalance. Four scenarios were simulated with the mass density of one blade adjusted by -1%, +2%, -3%, and +4%; while the mass densities of the other two blades were unchanged. Here the negative sign indicates a decrease of the mass density and the positive sign indicates an increase of the mass density. The proposed current frequency demodulation method and 1P-invariant PSD method were applied for the baseline case and the four blade imbalance scenarios. The base frequency was chosen to be 3 Hz (i.e., 180 rpm) and the base value of the down-sampling step size  $L$  was 20. Therefore, the variable characteristic frequency of 1P (2 to 4 Hz) of the blade imbalance faults in the estimated shaft frequency signal was converted to a constant value of 3 Hz. The results are compared in Figs. 5.3 and 5.4. It is clearly shown that in the blade imbalance scenarios excitations are evident at 1P, which is fixed at 3 Hz by using the proposed method. The imbalance is caused by an eccentric mass rotating with a frequency of 1P. The shaft rotating frequency is affected by the imbalance in blades and also vibrates with a frequency of 1P. Furthermore, Fig. 5.4 shows that the magnitude of the excitation at 1P increases with the increase of the degree of blade imbalance. On the other hand, no excitation is observed at 1P frequency in the PSD curve for the wind turbine with healthy blades.

In order to simulate aerodynamic asymmetry faults of the wind turbine, the pitch angle of one blade was adjusted by -2 degree, +4 degree, -6 degree, and +8 degree; while the pitch angles of the other two blades were unchanged at 11.44 degree. Figs. 5.5, 5.6 and 5.7 compare the 1P-invariant PSD of the estimated shaft rotating frequency generated by the proposed method for the wind turbine in the four aerodynamic asymmetry scenarios against the baseline case. Again, the variable 1P frequency was converted to a constant value of 3 Hz by using the proposed method. Excitations appear at both 1P and 2P frequencies in the four aerodynamic asymmetry scenarios, which agree with the theoretical analysis in section II. Moreover, the magnitudes of the excitations at the characteristic frequencies in the PSD plot become more significant when the degree of aerodynamic asymmetry becomes greater.

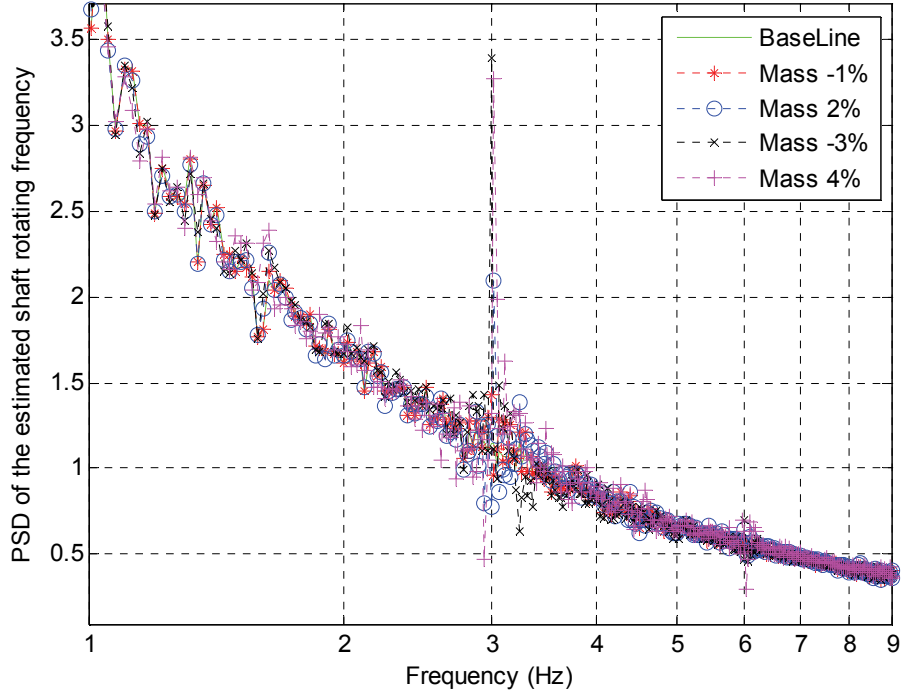


Fig. 5.3: Comparison of the 1P-invariant PSD of the estimated shaft rotating frequency for the blade imbalance scenarios against the baseline case in a wide frequency range.

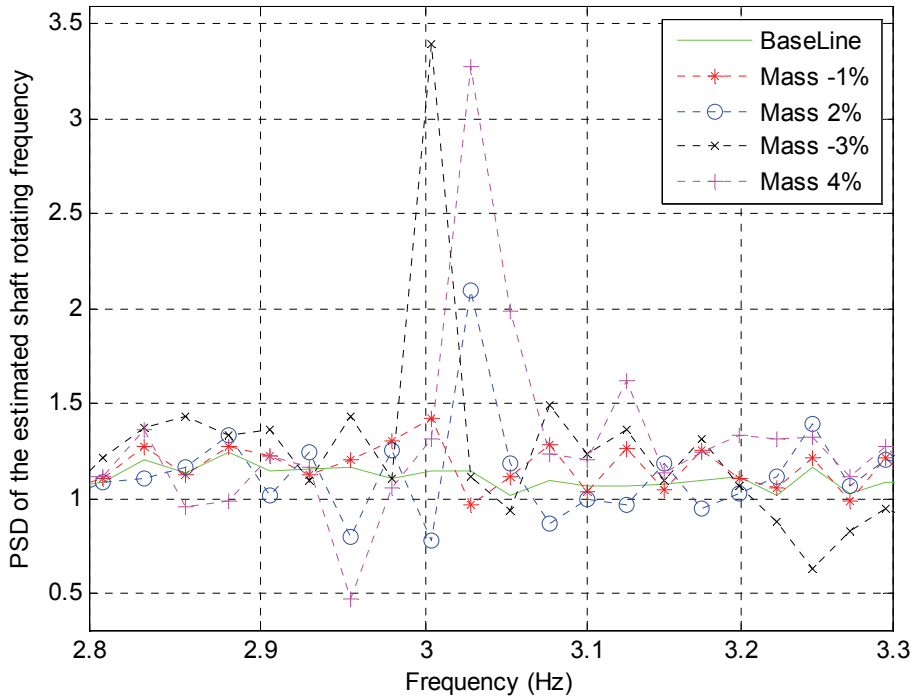


Fig. 5.4: Comparison of the 1P-invariant PSD of the estimated shaft rotating frequency for the blade imbalance scenarios against the baseline case in a frequency range around 1P.

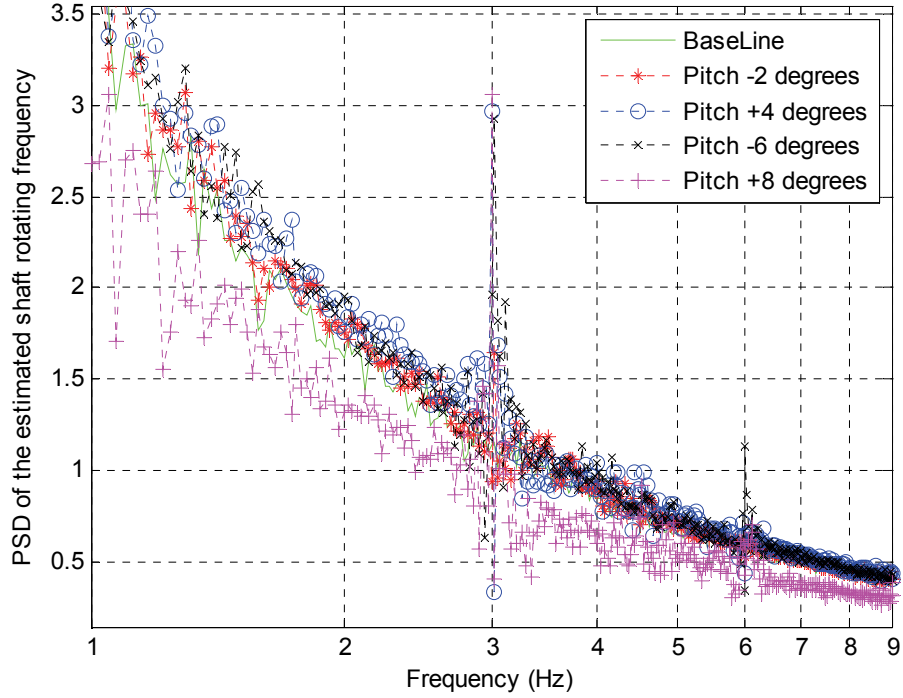


Fig. 5.5: Comparison of the 1P-invariant PSD of the estimated shaft rotating frequency for the aerodynamic asymmetry scenarios against the baseline case in a wide frequency range.

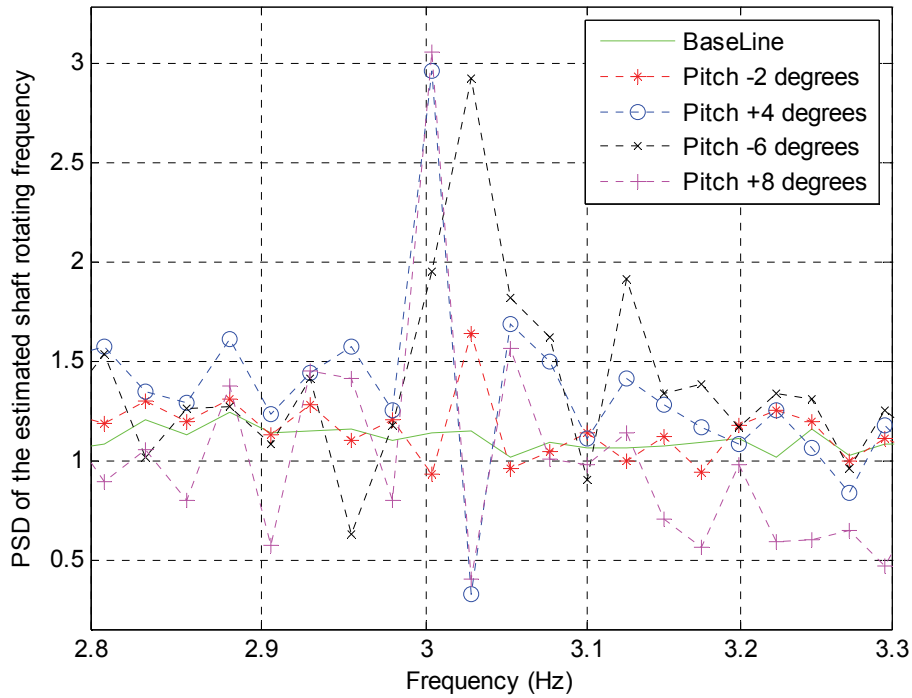


Fig. 5.6: Comparison of the 1P-invariant PSD of the estimated shaft rotating frequency for the aerodynamic asymmetry scenarios against the baseline case in a frequency range around 1P.

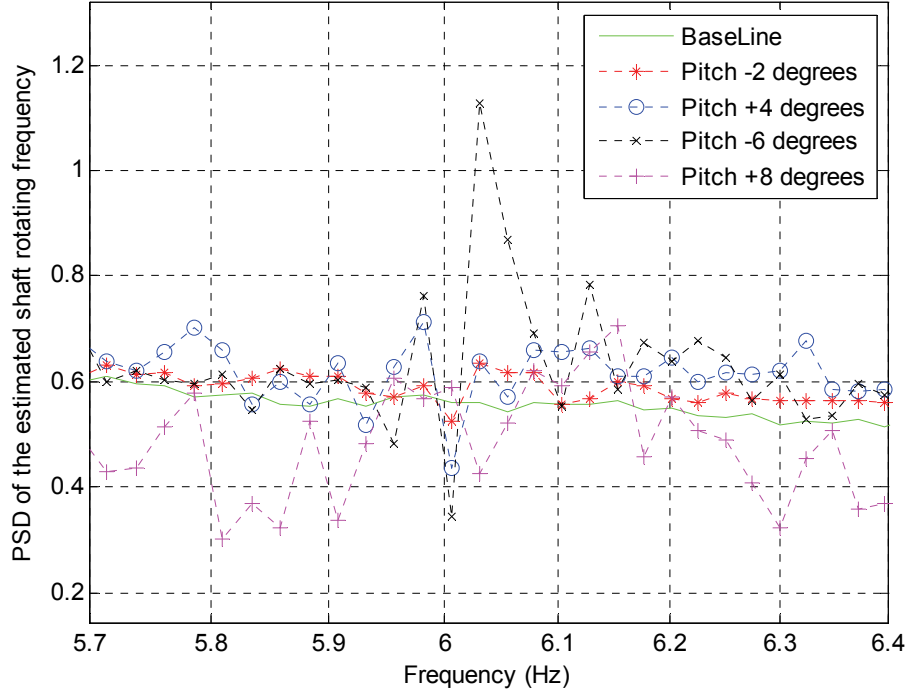


Fig. 5.7: Comparison of the 1P-invariant PSD of the estimated shaft rotating frequency for the aerodynamic asymmetry scenarios against the baseline case in a frequency range around 2P.

### 5.3 Experimental Study of Imbalance Fault Detection

A 160-W Southwest Windpower Air Breeze direct-drive WTG was used for experimental studies. The generator has six pole pairs. The experimental system setup has been described in Section 4.2. The length of each current and vibration record is 60 s.

#### 5.3.1 Detection of Blade Imbalance

To create a blade imbalance, additional masses were added close to the tip of a blade of the WTG, as shown in Fig. 5.8. The mass of a healthy blade was measured to be 181 g. Two sets of experiments were performed. In the first set of experiments, four blade imbalance scenarios were tested by adding a mass of 2.3 g, 4.5 g, 6.8 g, and 9 g, respectively, to a blade. Therefore, the weight of the blade was increased by 1.25%, 2.5%, 3.75%, and 5%, respectively. During the experiments, the WTG was operated at variable speed in the range of 6-13 Hz, which is the variable 1P frequency.

The proposed method was applied to obtain the 1P-invariant PSD of the measured WTG current for the four blade imbalance scenarios and the baseline case. In the proposed method, the base frequency  $f_b$  was chosen to be 10 Hz. Due to current frequency modulation with the 1P frequency, the fault characteristic frequencies should be  $60\text{Hz} \pm 1\text{P}$ , which are 50 Hz and 70 Hz since the variable 1P frequency has been converted to a constant value of 10 Hz. The results are compared in Figs. 5.9 and 5.10, where excitations are observed at 50 Hz and 70 Hz only in the

worst 5% blade imbalance scenario, but are not clearly observed in other blade imbalance scenarios, because the fault characteristic frequencies in the current signal are too close to the 60 Hz fundamental frequency component and, therefore, are masked by the sidebands of the fundamental frequency component in the PSD spectrum.



Fig. 5.8: A blade with an additional mass to create a blade imbalance fault.

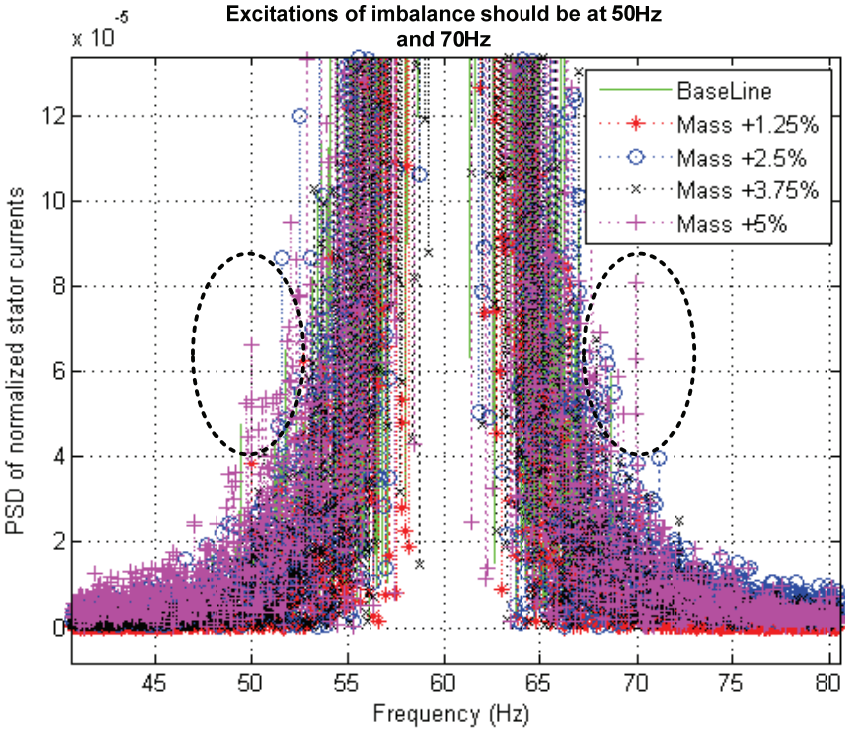


Fig. 5.9: Comparison of the 1P-invariant PSD of the current signal for the blade imbalance scenarios against the baseline case in a wide frequency range.

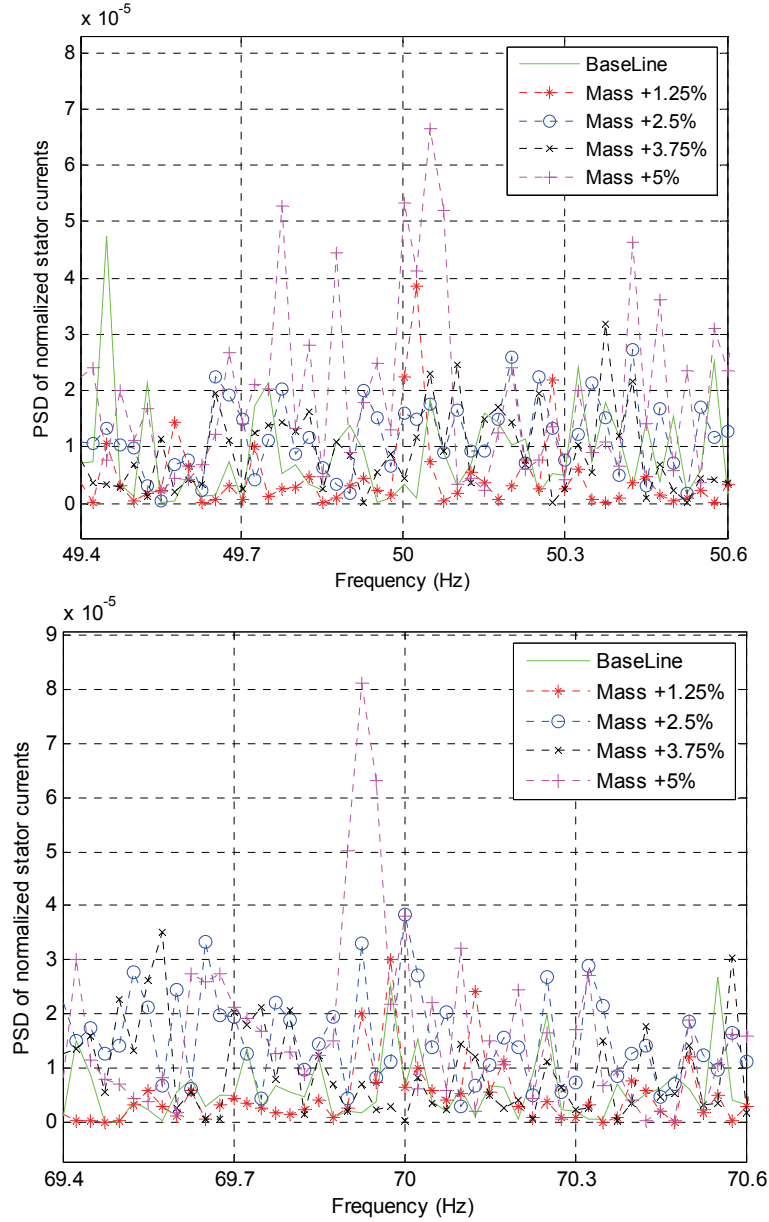


Fig. 5.10: Comparison of the 1P-invariant PSD of the current signal for the blade imbalance scenarios against the baseline case around 50 Hz and 70 Hz.

The current frequency demodulation method was applied to estimate the shaft rotating frequency of the wind turbine, whose PSD was then calculated by using the standard PSD analysis directly without using the up-sampling and down-sampling algorithms in the proposed 1P-invariant PSD method. The results are compared in Fig. 5.11 for the blade imbalance scenarios against the baseline case. The PSD of the estimated shaft frequency excites at the 1P frequency in the range of 6-13 Hz in the blade imbalance scenarios. However, it is difficult to quantify and evaluate the blade imbalance faults by using these results due to the variation of the 1P frequency component. Furthermore, if interferences are present near the 1P frequency, it will be difficult to identify fault signatures from the interferences by using the standard PSD analysis.

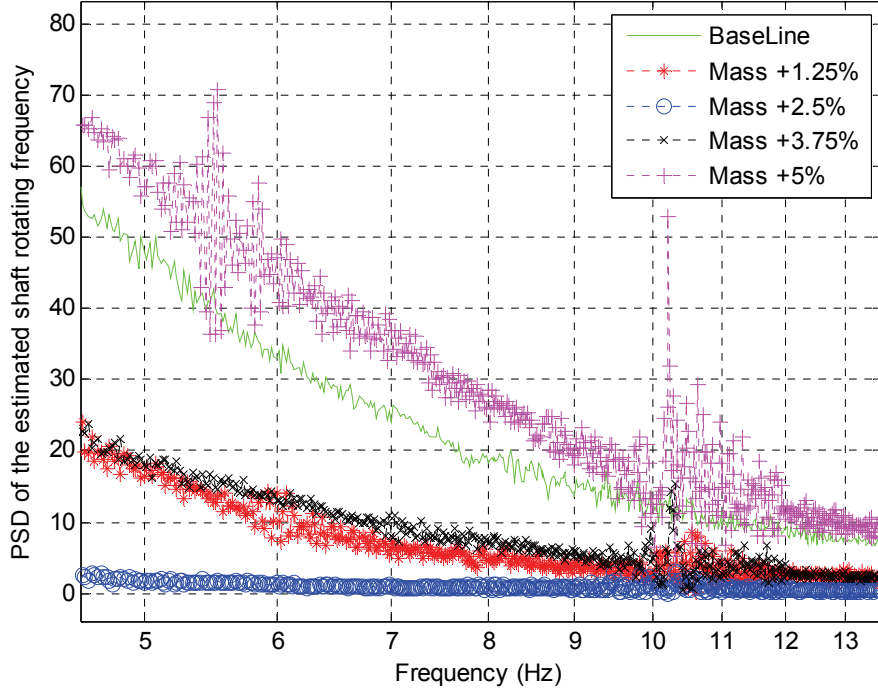


Fig. 5.10: Comparison of the PSD of the estimated shaft rotating frequency obtained directly from the standard PSD analysis for the blade imbalance scenarios against the baseline case.

In the second set of experiments, four blade imbalance scenarios were tested by adding a mass of 1.8 g, 3.6 g, 5.4 g, and 7.2 g, respectively, to a blade. Therefore, the weight of the blade was increased by 1%, 2%, 3% and 4%, respectively. The proposed method was applied to obtain the 1P-invariant PSD of the estimated shaft rotating frequency of the WTG for the four blade imbalance scenarios and the baseline case. In the 1P-invariant PSD method, the base frequency  $f_b$  was chosen to be 10 Hz. The results are compared in Figs. 5.11 and 5.12, where excitations are clearly observed at the fixed 1P frequency of 10 Hz in the blade imbalance scenarios. Thus, the magnitude of this excitation provides an effective signature for detecting blade imbalance faults. The greater the magnitude of the excitation appears at the 1P frequency, the higher degree of the blade imbalance. Therefore, the proposed method can not only identify but can also quantify the degree of blade imbalance of the WTG.

The proposed 1P-invariant PSD method was also applied the vibration measurements of the WTG for the four blade imbalance scenarios and the baseline case, where the base frequency  $f_b$  was also chosen to be 10 Hz. The results are shown in Figs. 5.13 and 5.14, which are similar to the results of using the current frequency demodulated signal, i.e., the estimated shaft rotating frequency. The results of Figs. 5.11-5.14 clearly demonstrate that the proposed current-based technologies achieved comparable performance as the traditional vibration-based methods for wind turbine blade imbalance fault detection.

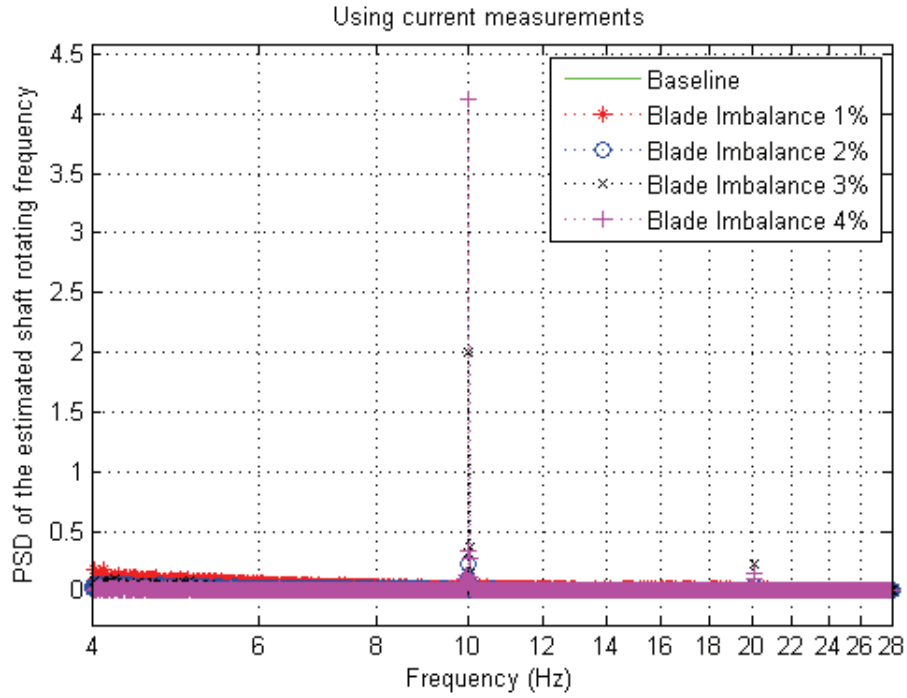


Fig. 5.11: Comparison of the 1P-invariant PSD of the estimated shaft rotating frequency for the blade imbalance scenarios against the baseline case in a wide frequency range.

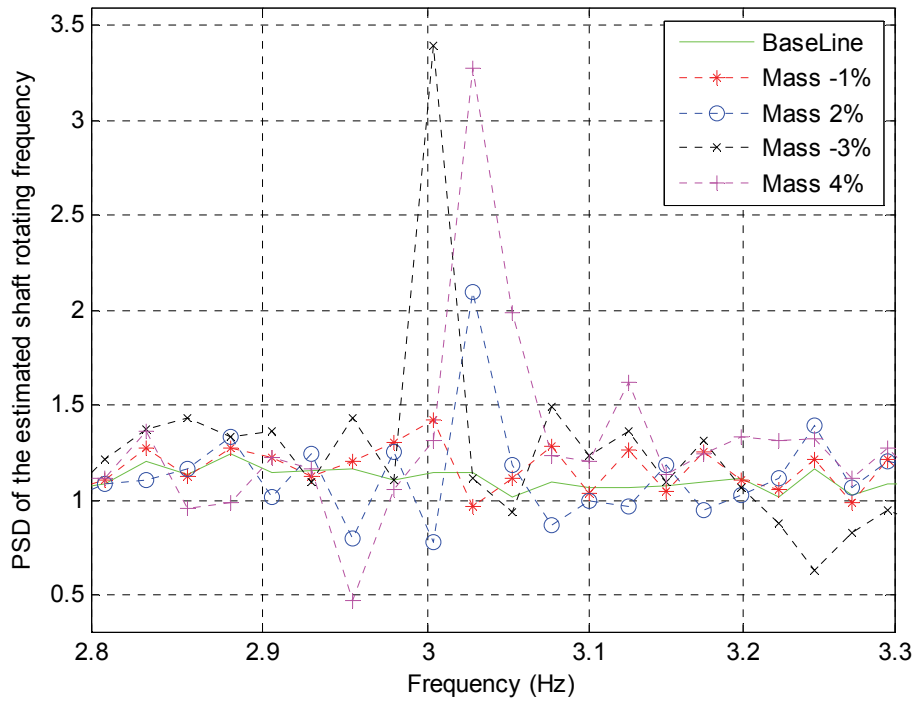


Fig. 5.12: Comparison of the 1P-invariant PSD of the estimated shaft rotating frequency for the blade imbalance scenarios against the baseline case in a frequency range around 1P.

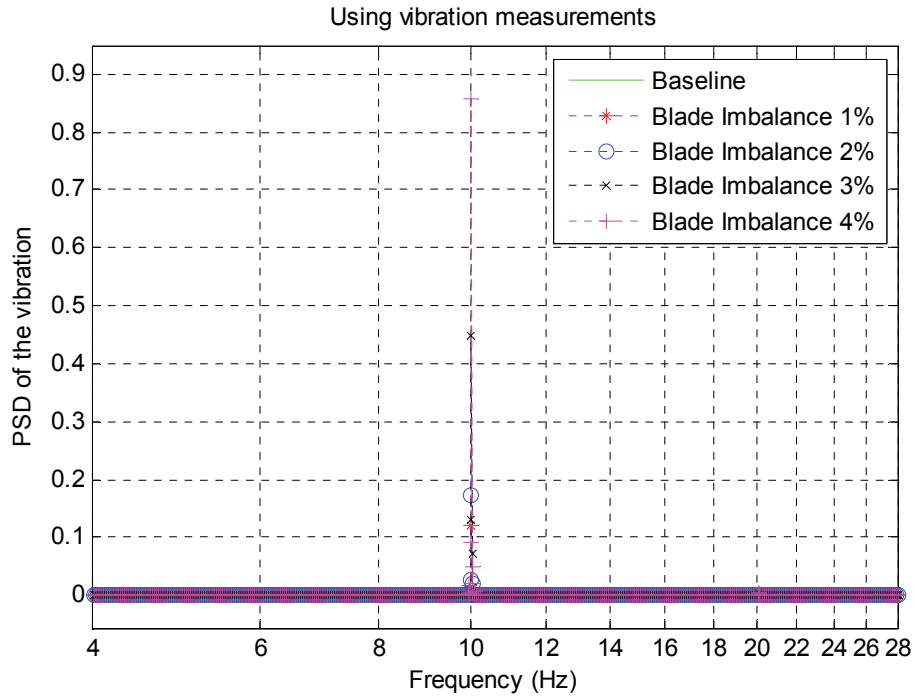


Fig. 5.13: Comparison of the 1P-invariant PSD of the vibration signal for the blade imbalance scenarios against the baseline case in a wide frequency range.

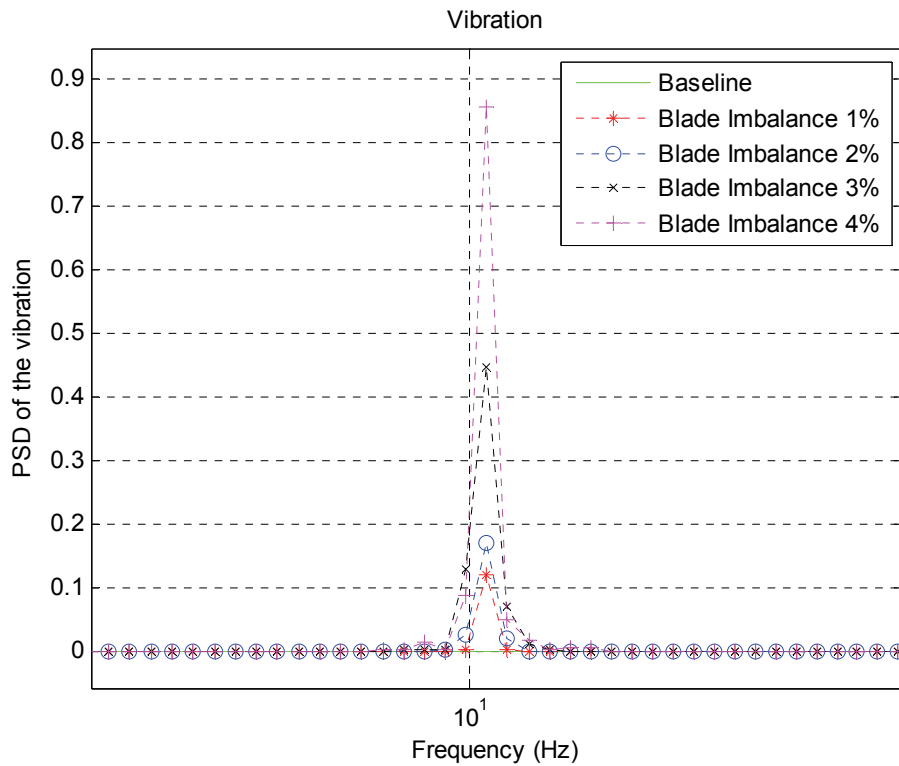


Fig. 5.14: Comparison of the 1P-invariant PSD of the vibration signal for the blade imbalance scenarios against the baseline case in a frequency range around 1P.

### 5.3.2 Detection of Bent Blades

A bent blade is a blade of a WTG that twists flapwise or edgewise, as illustrated in Fig. 5.15. A bent blade also generates an imbalance fault in the WTG. During the experiments, one blade of the Air Breeze wind turbine was bent edgewise at 2, 4, and 6 degree, respectively. Figs. 5.16 and 5.17 compare the 1P-invariant PSD of the estimated shaft frequency of the WTG for the edgewise bent blade scenarios against the baseline case by using the proposed current frequency demodulation method and 1P-invariant PSD method with the same base frequency  $f_b$  as in the blade imbalance study. As shown in Figs. 5.16 and 5.17, an excitation appears at a fixed frequency of 1P (10 Hz) in the PSD plots of the bent blade cases. The magnitude of the 1P excitation provides an effective signature for detecting and quantifying the bent blade faults.

Since the wind turbine was operated in the wind tunnel during the experiments and there was no wind shear or yaw error in the wind tunnel, as shown in Figs. 5.11 and 5.16, there is no excitation at 2P frequency in the experimental results, which is another characteristic frequency of aerodynamic asymmetries.

In another set of experiments, one blade of an Air Breeze wind turbine was bended edgewise in two different directions: forward and backward, as shown in Fig. 5.18; while the other two blades were unchanged. Figs. 5.19 and 5.20 show the 1P-invariant PSD results for two bent blade cases against the baseline case using the current frequency demodulated signal (i.e., the estimated shaft rotating frequency) and the vibration signal, respectively, where again the variable 1P frequency was converted to a constant value of 10 Hz. Both the proposed current-based methods and the traditional vibration-based method are effective for detecting the edgewise bent blade faults. Moreover, the proposed current-based methods achieved comparable performance as the traditional vibration-based method for wind turbine bent blade fault detection.

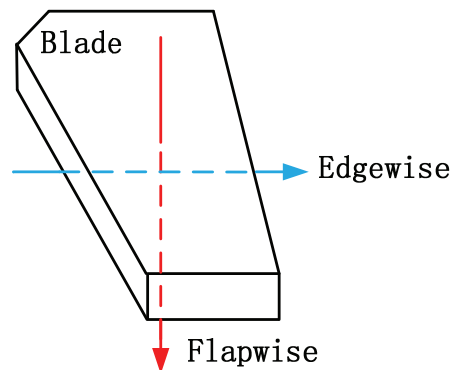


Fig. 5.15: A blade bended flapwise or edgewise.

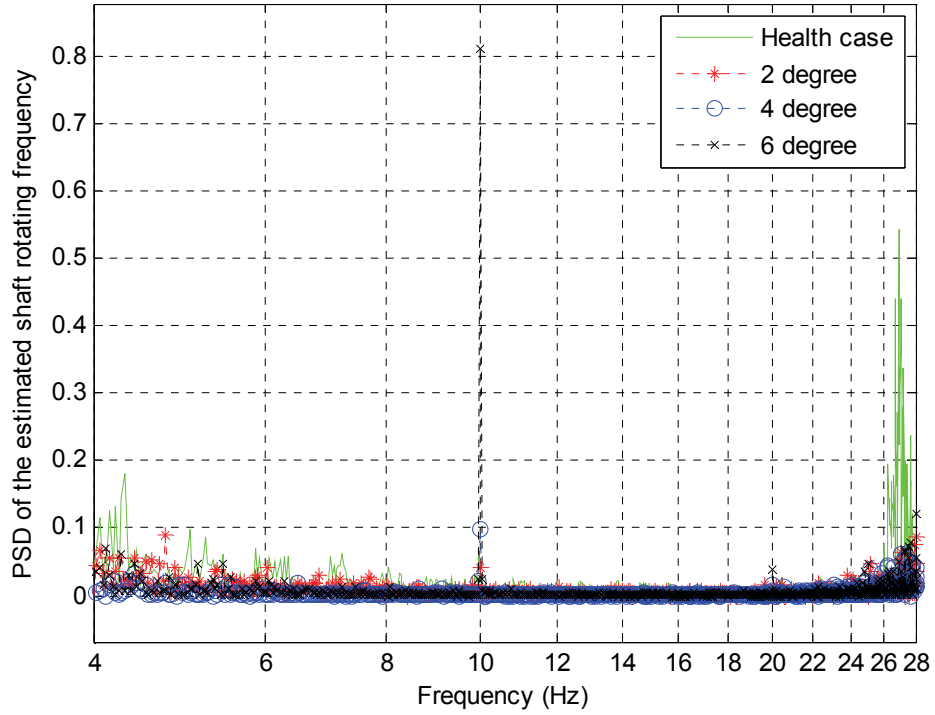


Fig. 5.16: Comparison of the 1P-invariant PSD of the estimated shaft rotating frequency for the edgewise bent blade scenarios against the baseline case in a wide frequency range.

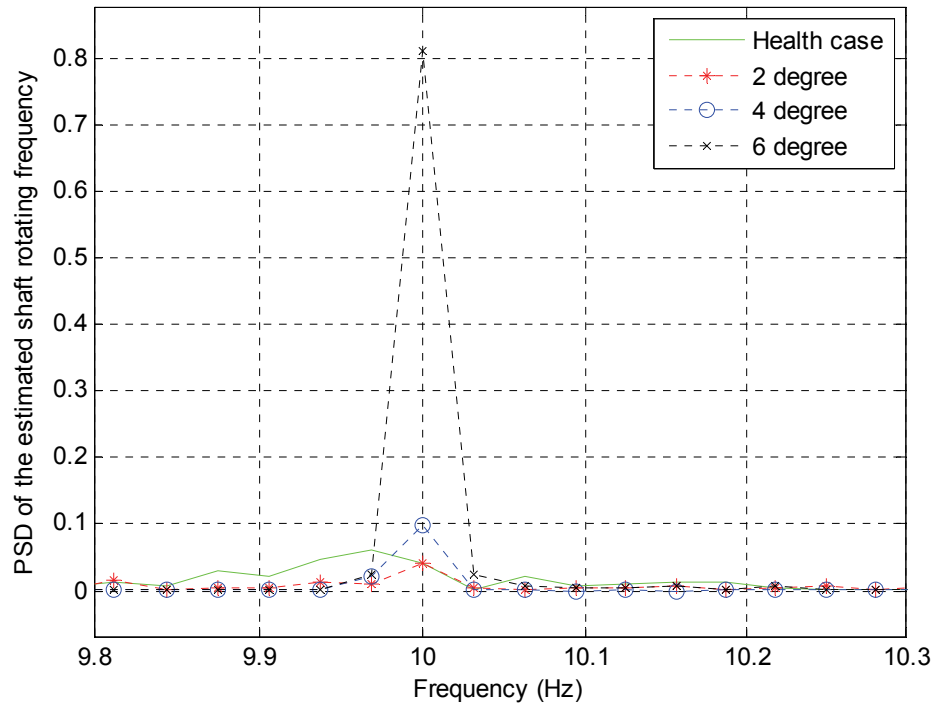


Fig. 5.17: Comparison of the 1P-invariant PSD of the estimated shaft rotating frequency for the edgewise bent blade scenarios against the baseline case in a frequency range around 1P.



Fig. 5.18: A blade of the Air Breeze wind turbine bended forward (left) and backward (right).

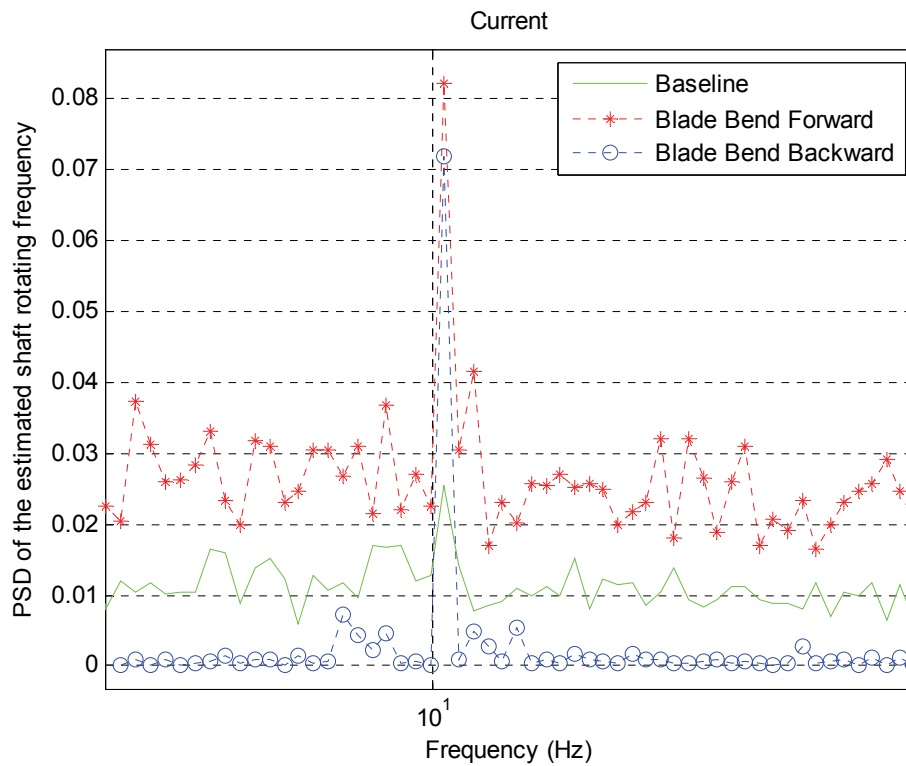


Fig. 5.19: Comparison of the 1P-invariant PSD of the estimated shaft rotating frequency for the flapwise bent blade scenarios against the baseline case in a frequency range around 1P.

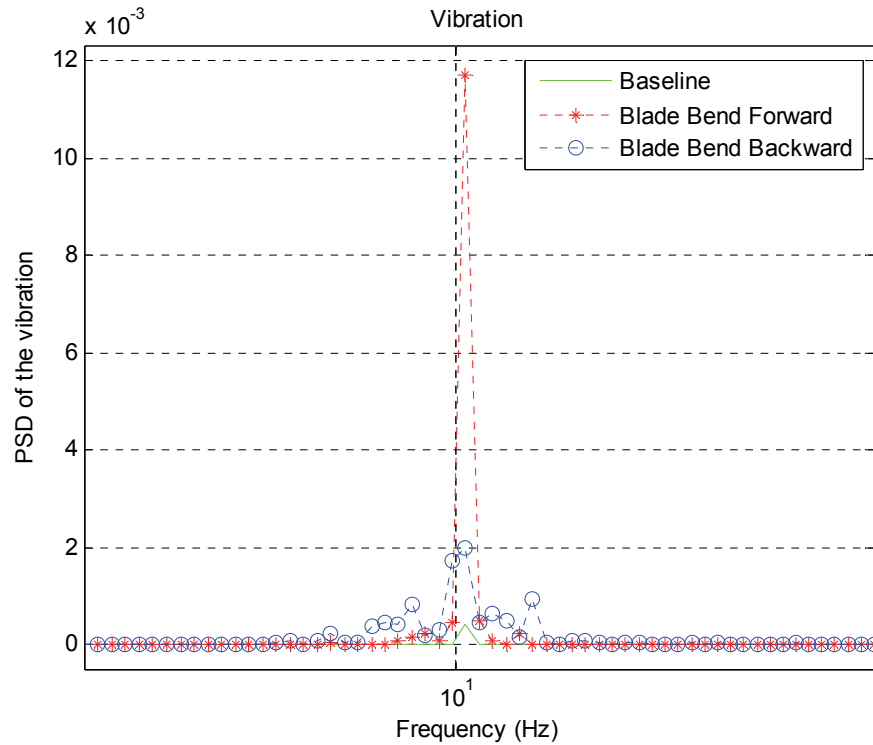


Fig. 5.20: Comparison of the 1P-invariant PSD of the vibration signal for the flapwise bent blade scenarios against the baseline case in a frequency range around 1P.

### 5.3.3 Detection of Aged Blade

In this test an Air Breeze wind turbine was equipped with an aged blade and two new blades. Fig. 5.21 compares the aged blade with a new blade. The aged blade has cracks and its surface becomes rough. The developed 1P-invariant PSD method was applied to both the current frequency demodulated signal and the vibration signal for aged blade detection; the results are shown in Figs. 5.22 and 5.23, respectively.



Fig. 5.21: Comparison of the aged blade with a new blade.

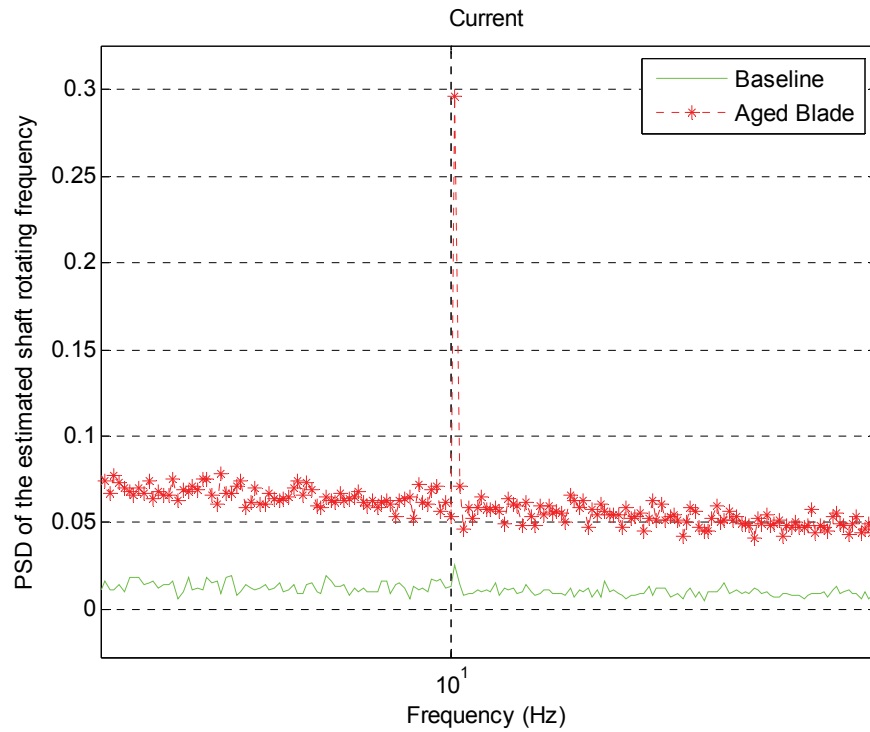


Fig. 5.22: Comparison of the 1P-invariant PSD of the estimated shaft rotating frequency for the aged blade case against the baseline case in a frequency range around 1P.

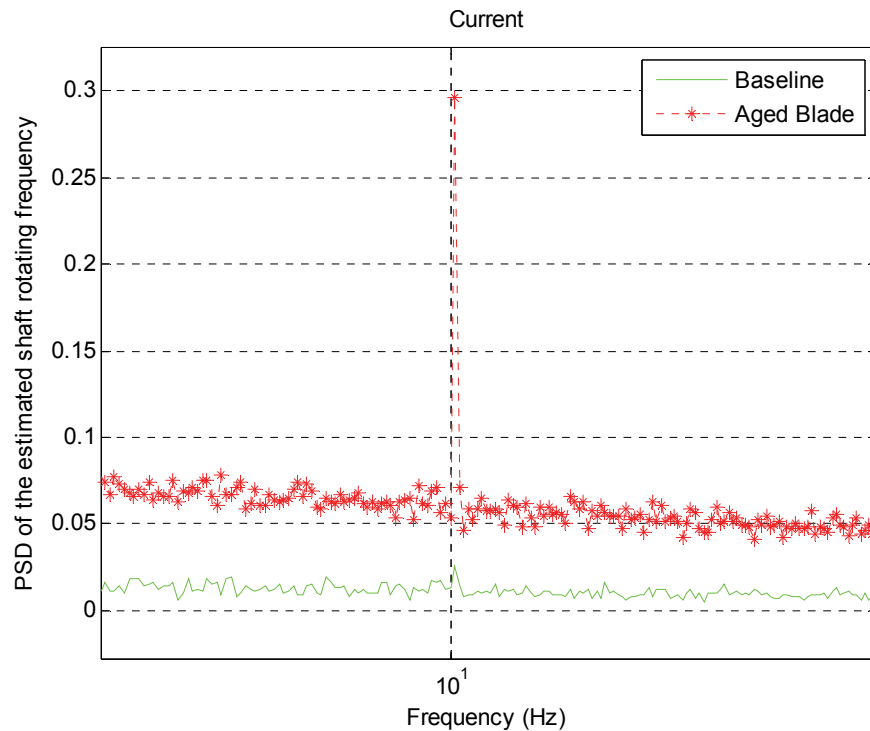


Fig. 5.23: Comparison of the 1P-invariant PSD of the vibration signal for the aged blade case against the baseline case in a frequency range around 1P.

#### 5.3.4 Detection of Blade Defects

In this set of experiments, a blade with two-point defects and a blade with four-point defects were created, as shown in Fig. 5.24. Each defected blade was used individually in the experiments; while other two blades of the Air Breeze wind turbine were unchanged in each experiment. Figs. 5.25 and 5.26 compare the 1P-invariant PSD results for an Air Breeze wind turbine in two blade defect cases against the baseline case using the current frequency demodulated signal and the vibration signal, respectively. Blade Defect 2 and Blade Defect 4 in the figures refer to a blade with two-point defects and a blade with four-point defects, respectively.



Fig. 5.24: Two defected blades used for experiments.

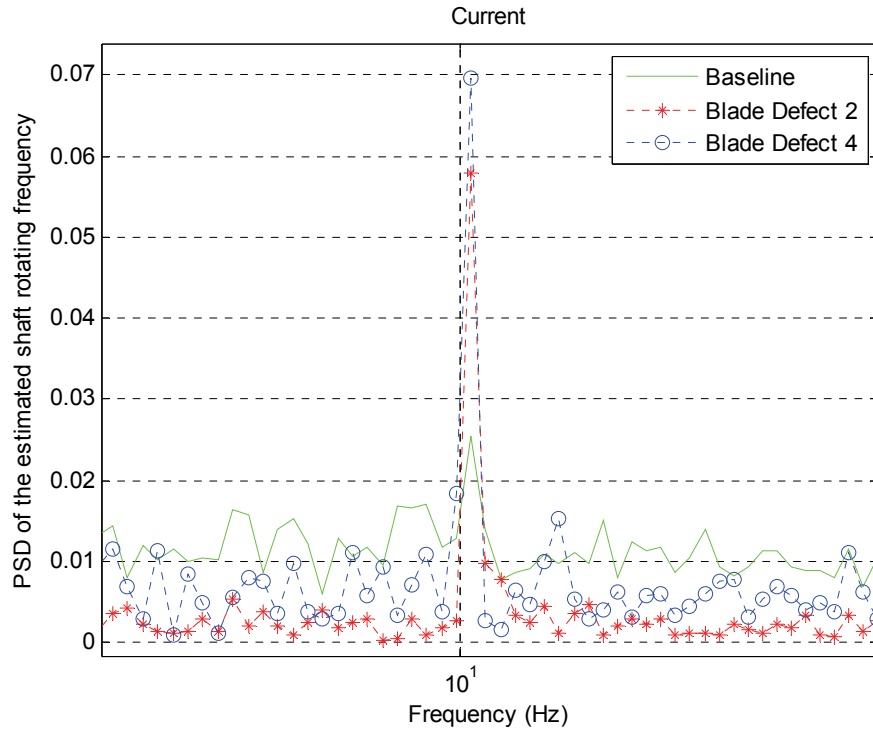


Fig. 5.25: Comparison of the 1P-invariant PSD of the estimated shaft rotating frequency for the blade defect cases against the baseline case in a frequency range around 1P.

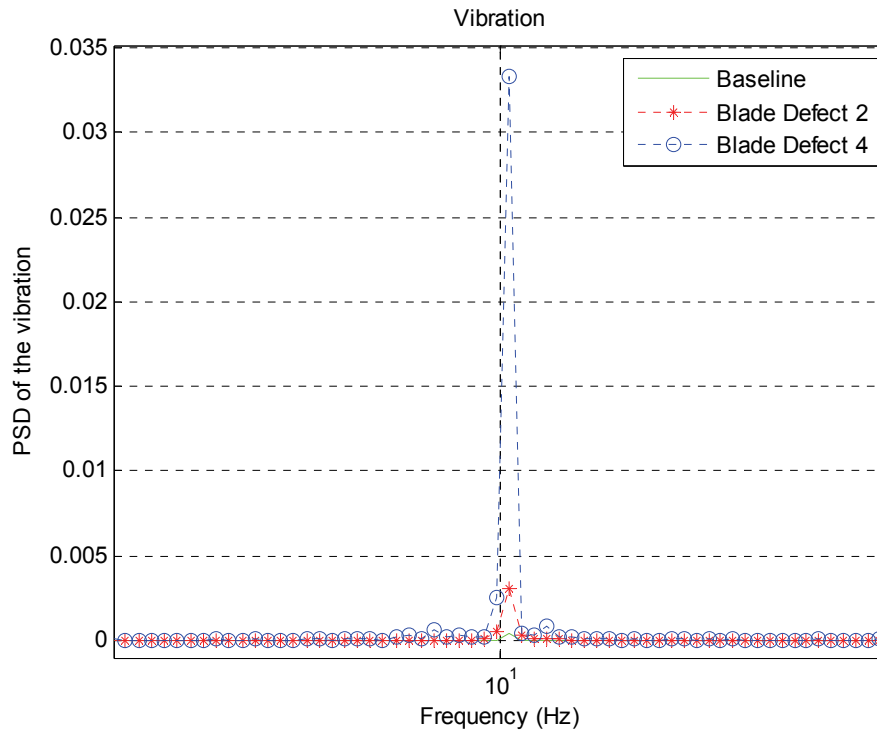


Fig. 5.26: Comparison of the 1P-invariant PSD of the vibration signal for the blade defect cases against the baseline case in a frequency range around 1P.

### 5.3.5 Detection of Generator Magnet Damage

In this test, one of the rotor magnets of the generator of an Air Breeze wind turbine was broken, as shown in Fig. 5.27. Figs. 5.28 and 5.29 compare the 1P-invariant PSD results for an Air Breeze wind turbine in the magnet damage case against the baseline case using the current frequency demodulated signal and the vibration signal, respectively.



Fig. 5.27: A rotor with a damaged magnet of the generator of an Air Breeze wind turbine.

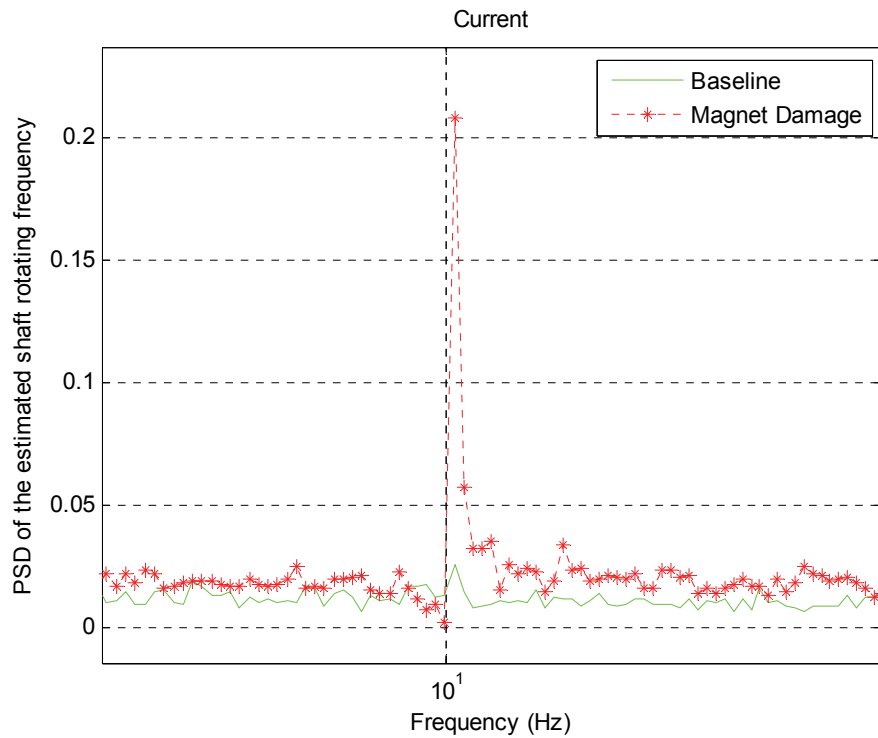


Fig. 5.28: Comparison of the 1P-invariant PSD of the estimated shaft rotating frequency for the magnet damage case against the baseline case in a frequency range around 1P.

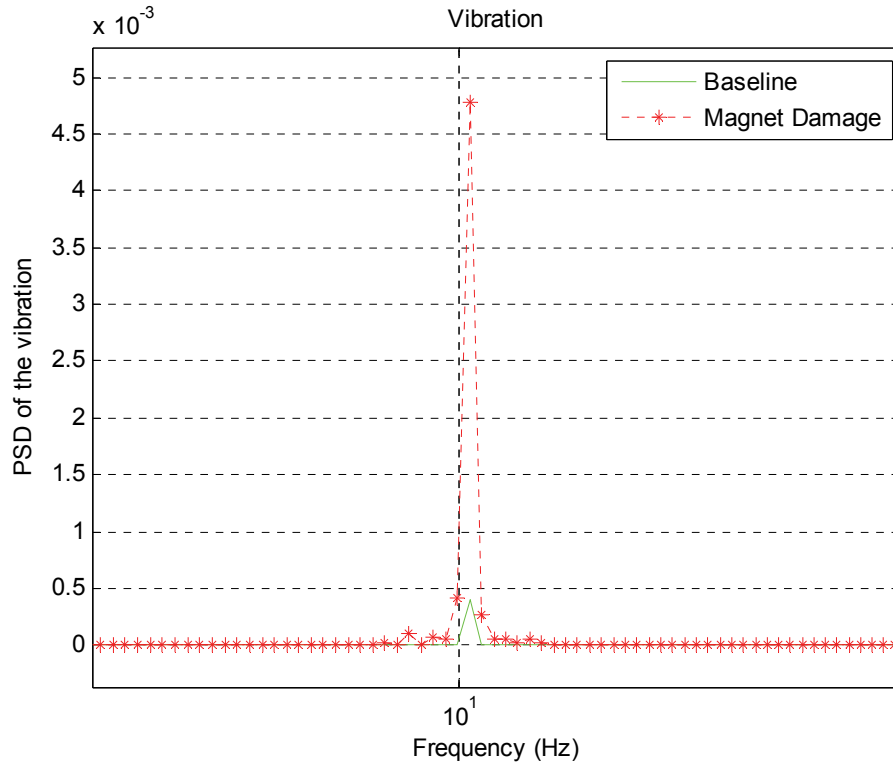


Fig. 5.29: Comparison of the 1P-invariant PSD of the vibration signal for the magnet damage case against the baseline case in a frequency range around 1P.

The results in Sections 5.3.3-5.3.5 clearly show that the proposed 1P-invariant method is effective to detect these wind turbine faults by using both current and vibration measurements. The proposed current-based fault detection method achieved comparable performance as the traditional vibration-based method for detection of various imbalance faults for wind turbines.

## 6. WIND TURBINE BEARING FAULT DETECTION

Bearing faults constitute a significant portion of all faults in wind turbine generators (WTGs). The experience feedback from the wind energy industry corroborates that bearing failure is one of the typical failures in WTGs [3], [39]. Repairing or replacing a faulted bearing requires additional cost and can cause significant downtime. For instance, failure of a \$1,500 bearing, if not repaired or replaced timely, could result in a \$100,000 gearbox replacement, a \$50,000 generator rewind, and \$70,000 in expenses to replace other failed components [39]. According to General Electric (GE) Energy [3], a \$5,000 bearing replacement can easily turn into a \$250,000 project involving cranes, service crew, gearbox replacement, and generator rewind, not to mention the downtime loss of power generation. Therefore, it is highly desired to detect bearing faults and repair or replace the faulted bearing(s) to prevent catastrophic damages and reduce the downtime of WTG systems.

### 6.1 The Characteristic Frequencies of Single-Point Bearing Faults

#### 6.1.1 Types of Single-Point Bearing Faults

According to different stages of the fault development process, bearing faults can be categorized into two types [43]: 1) single-point defect, which is defined as a single and localized defect on an otherwise relatively undamaged bearing surface, and 2) generalized roughness, which is a type of fault where the condition of a bearing surface has degraded considerably over a large area and become rough, irregular, or deformed.

According to [16], [44], the fault characteristic frequencies of a ball bearing in vibration measurements can be computed as functions of the geometry and rotating frequency of the bearing.

$$f_i = 0.5 \cdot N_B \cdot f_r \cdot (1 + D_b \cdot \cos\theta / D_c) \quad (6-1)$$

$$f_o = 0.5 \cdot N_B \cdot f_r \cdot (1 - D_b \cdot \cos\theta / D_c) \quad (6-2)$$

$$f_b = 0.5 \cdot f_r \cdot (D_c / D_b) \cdot [1 - (D_b \cdot \cos\theta / D_c)^2] \quad (6-3)$$

$$f_c = 0.5 \cdot f_r \cdot (1 - D_b \cdot \cos\theta / D_c) \quad (6-4)$$

where  $f_i$  is the characteristic frequency of bearing inner-race faults;  $f_o$  is the characteristic frequency of bearing outer-race faults;  $f_b$  is the characteristic frequency of bearing ball faults;  $f_c$  is the characteristic frequency of bearing cage faults;  $f_r$  is the rotating frequency of the bearing;  $N_B$  is the number of balls in the bearing;  $D_b$  is the ball diameter;  $D_c$  is the pitch diameter; and  $\beta$  is the ball contact angle, which is normally zero. The schematic diagram of a ball bearing with 8 balls is given in Fig. 6.1.

The excitations of a bearing fault appear not only in the frequency spectrum of WTG vibration measurements, but also in the frequency spectrum of WTG shaft rotating frequency signals. Therefore, the excitations at  $f_i$ ,  $f_o$ ,  $f_b$ , and  $f_c$ , in the frequency spectrum of shaft rotating frequency signals are signatures for bearing fault detection.

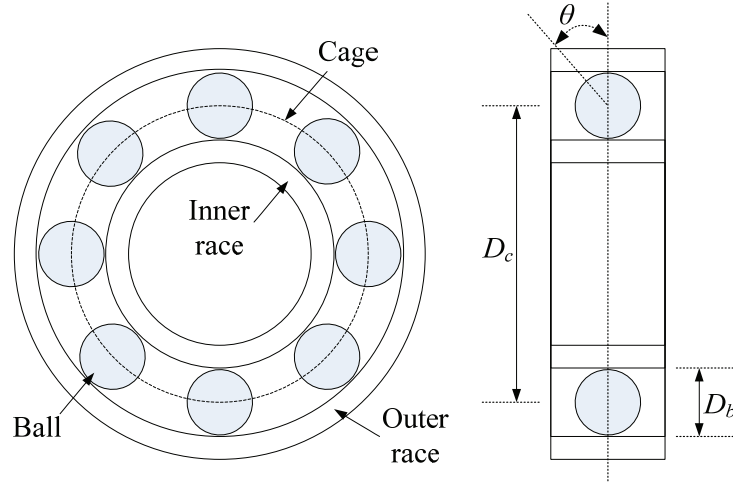


Fig. 6.1: Schematic diagram of a ball bearing.

### 6.1.2 Bearing Fault Signatures in Stator Current Signals

To apply current signals for WTG bearing fault detection, the influence of bearing faults on the WTG current signals needs to be modeled. The most frequently used model is given in [45] for induction machine bearing fault detection. Reference [46] extended the result of [45] by taking into account both the radial rotor movement and the shaft torque variation of electric machines. The stator current signals are modulated by the characteristic frequency  $f_{fault}$  of a bearing fault in vibration measurements, where  $f_{fault}$  is one of the bearing fault characteristic frequencies given in (6.1)-(6.4) [45], [46]. The characteristic frequencies of bearing single-point defects in the modulated stator current signals are summarized in Table 6.1, where  $l = 1, 2, \dots$ ;  $f_{c,i}$ ,  $f_{c,o}$ ,  $f_{c,b}$ , and  $f_{c,c}$  are the characteristic frequencies of an inner-race defect, outer-race defect; ball defect; and cage defect, respectively; and  $f_1$  is the fundamental frequency of the current signal. The harmonics of current signals are also modulated by the bearing fault characteristic frequencies in vibration measurements. Since the harmonics of current signals have much lower magnitude than the fundamental-frequency component, the excitations at the harmonics due to bearing faults are minor and are not listed here.

Table 6.1: Characteristic frequencies of single-point bearing faults in WTG current signals

	Radial rotor movement [45]	Radial rotor movement [46]	Shaft torque variation [46]
Inner-race defect	$f_{c,i} = f_1 \pm l \cdot f_i$	$f_{c,i} = f_1 \pm f_r \pm l \cdot f_i$	$f_{c,i} = f_1 \pm l \cdot f_i$
Outer-race defect	$f_{c,o} = f_1 \pm l \cdot f_o$	$f_{c,o} = f_1 \pm l \cdot f_o$	$f_{c,o} = f_1 \pm l \cdot f_o$
Ball defect	$f_{c,b} = f_1 \pm l \cdot f_b$	$f_{c,b} = f_1 \pm f_c \pm l \cdot f_b$	$f_{c,b} = f_1 \pm l \cdot f_b$
Cage defect	$f_{c,c} = f_1 \pm l \cdot f_c$	N/A	N/A

## 6.2 Single-Point Bearing Fault Detection

### 6.2.1 WTG with Healthy Bearings

A baseline scenario was initially studied for the testing Air Breeze wind turbine with healthy bearings. The testing bearing is located between the rotors of the turbine and the generator, as shown in Fig 6.2. The Air Breeze PMSG wind turbine was operated with the rotating frequency in the range of 11 to 12 Hz, which leads to 66 to 72 Hz fundamental frequency in the stator current signals. The length of the stator current measurement is 10 second. The measured stator current was demodulated and analyzed by using the proposed method. The 1P-invariant PSDs of the frequency and amplitude demodulated signals of the stator current are plotted in Figs. 6.3 and 6.4, respectively, where the variable shaft rotating frequency from 11 to 12 Hz was converted to a constant value of 10 Hz by using the 1P-invariant PSD method. In Fig. 6.3, there are excitations at the frequencies of 10 Hz and 30 Hz besides the DC component in the 1P-invariant PSD of the frequency demodulated signal  $f_{1,e}$  of the stator current. The first excitation frequency is the 1P frequency, which was created by imbalance of the WTG, including shaft imbalance and rotor eccentricity [9]. WTGs are inevitably subjected to a certain degree of imbalance due to manufacturing and construction errors, icing, deformation, etc. The second excitation at 3P frequency was generated by the effect of yaw error, wind shear, or tower shadow of wind turbines with three blades [12]. In Fig. 6.3, besides the excitations appear at 1P and 3P frequencies, the amplitude demodulated signal of the stator current also contains 20 Hz or 2P frequency component. This is because the imbalance of the WTG modulates the amplitude of the stator current signal. The squared current signal contains the second harmonic of the 1P frequency as explained in (3-40), when  $f_{fault}$  equals to 1P frequency. The terms containing  $2\theta(t)$  of  $C_s^2$  in (3-40) were filtered out by using the 1P-invariant PSD method and do not appear in Fig. 6.4.

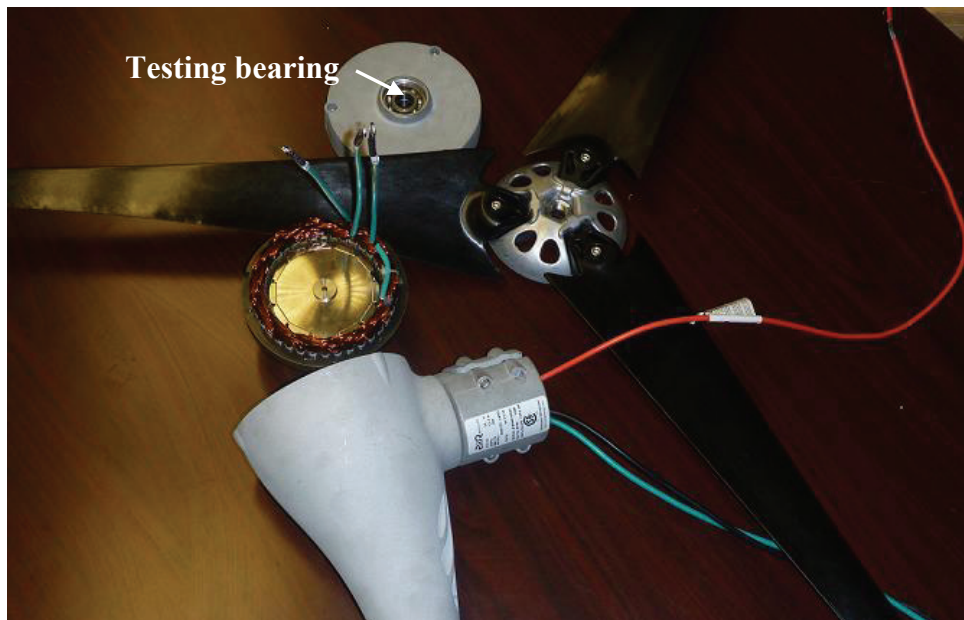


Fig. 6.2: The testing bearing and WTG.

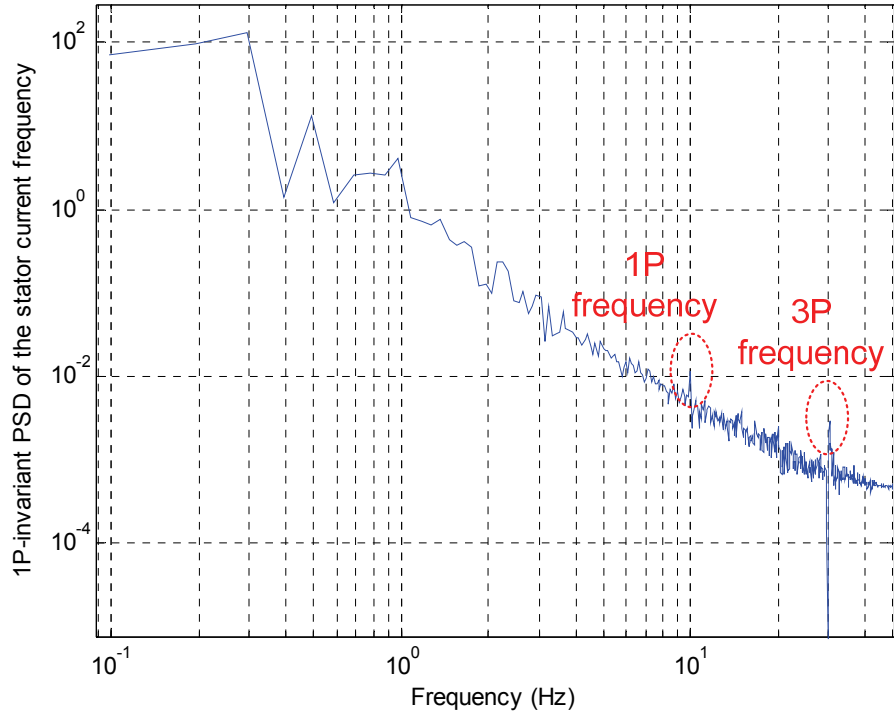


Fig. 6.3: The 1P-invariant PSD of the frequency demodulated signal of the stator current in the healthy bearing case.

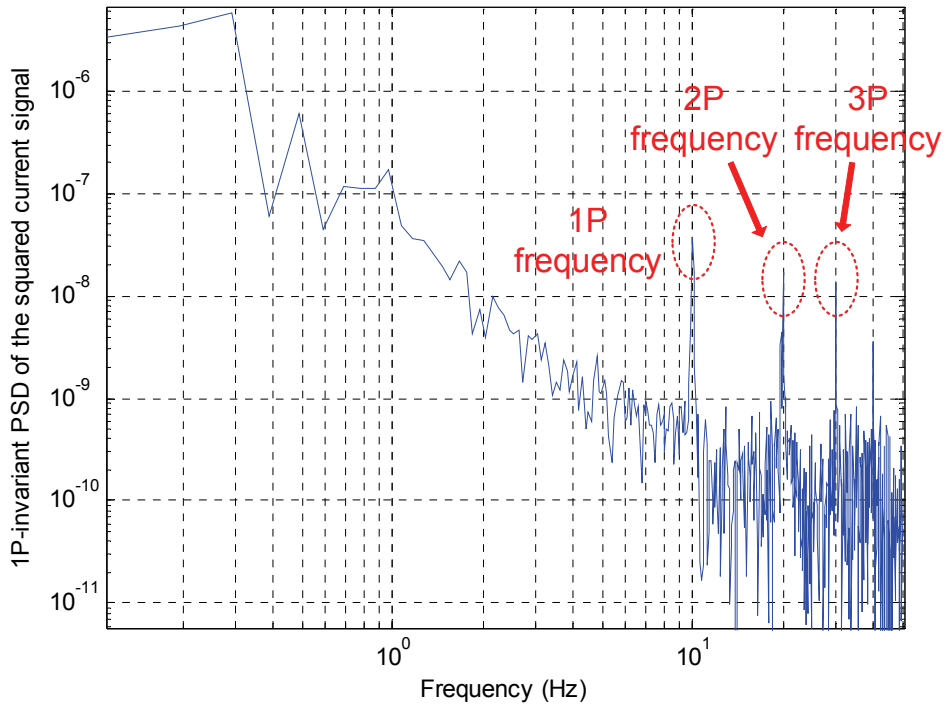


Fig. 6.4: The 1P-invariant PSD of the amplitude demodulated signal of the stator current in the healthy bearing case.

### 6.2.2 WTG with a Bearing Cage Broken Fault

In this test the testing bearing was pretreated by removing the lubricant oil. This generated a shaft torque variation in the testing WTG. The WTG has been operated with the variable rotating frequency in the range of 9 to 11 Hz in the wind tunnel for approximately 25 hours. The WTG stopped running at the end of the experiment due to the break of the bearing cage. Fig. 6.5 shows the testing bearing before and after the experiment.

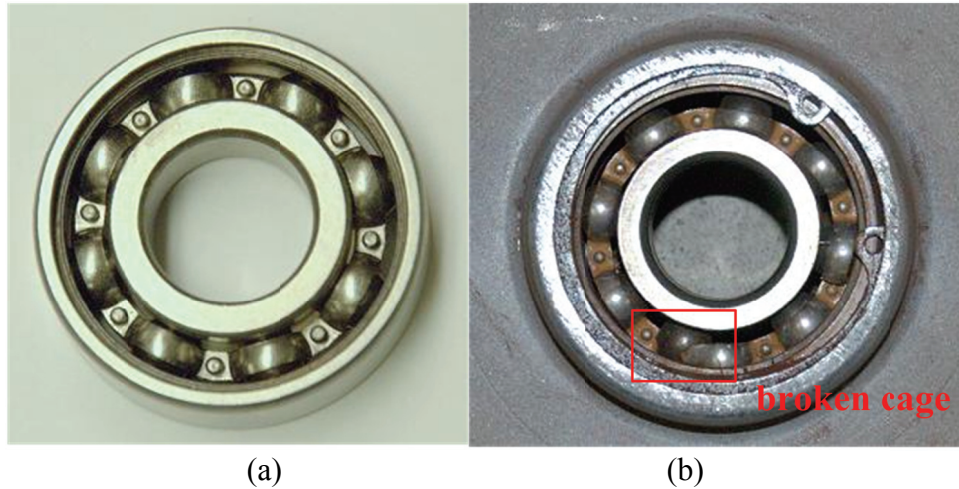


Fig. 6.5: Testing bearing: (a) is healthy before experiment and (b) with broken cage after experiment.

The 1P-invariant PSDs of the shaft rotating frequency signals estimated from the first (healthy bearing) and the last stator current records (bearing with cage fault) are compared in Fig. 6.6, where the variable 1P frequency in the range of 6 to 13 Hz was converted to a constant value of 10 Hz. As shown in Fig. 6.6, an excitation appears in the PSD of the estimated shaft rotating frequency signal at a fixed frequency of 4 Hz in the bearing cage fault case. This fault characteristic frequency is the same as the one calculated from (6.4) for the WTG operating with a constant shaft rotating frequency of 10 Hz. Thus, the excitation at 4 Hz in the 1P-invariant PSD of the estimated shaft rotating frequency signal is an effective signature for bearing cage fault detection. Moreover, the second-order harmonic of the excitation generated by the bearing cage fault can be found at the 8 Hz in Fig. 6.6.

The proposed impulse detection method was applied to extract the excitations in the 1P-invariant PSD for bearing cage fault detection. The length of the window,  $W$ , was chosen to be 101. A third-order median filter was designed for threshold calculation. The locally normalized PSD [i.e.,  $R(f)$ ] of the last record (bearing with cage fault) is plotted in Fig. 6.7. The threshold was calculated to be 0.11. The impulses appear at 4 Hz and 8 Hz, where the impulse at 4 Hz indicates the signature of a bearing cage fault; the impulse at 8 Hz is the second-order harmonic of the excitation generated by bearing cage fault.

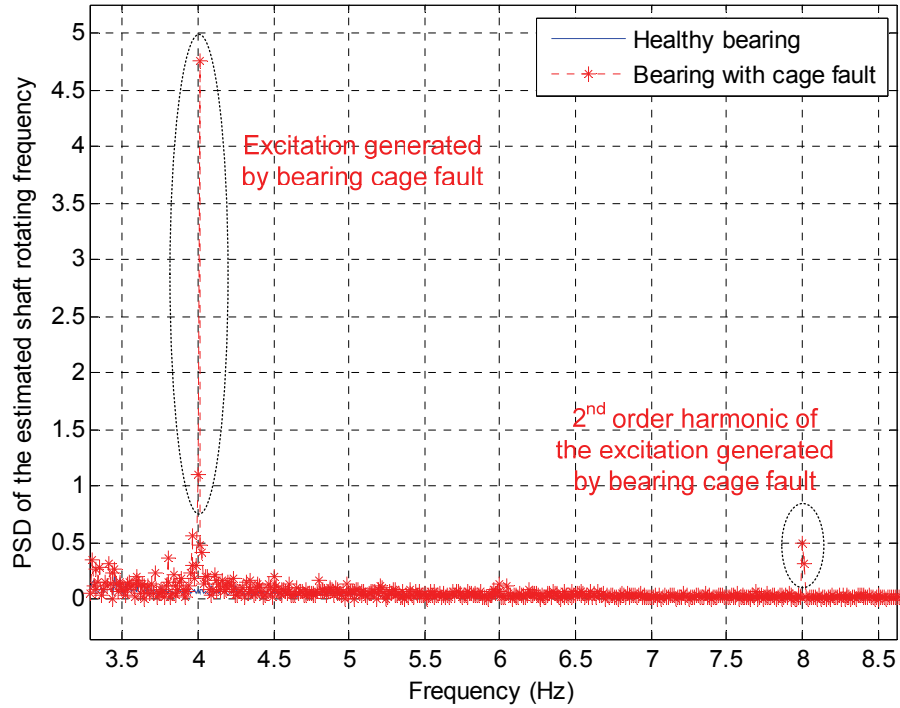


Fig. 6.6: Comparison of the 1P-invariant PSDs of the processed shaft rotating frequency signals estimated from the first and the last stator current records.

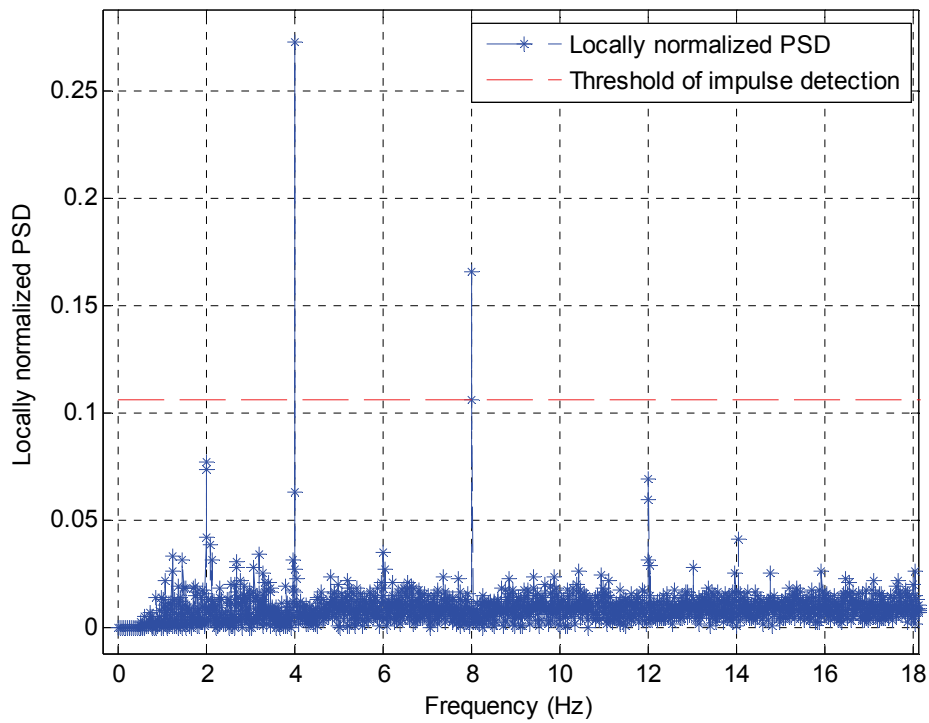


Fig. 6.7: Locally normalized PSD and threshold generated by the impulse detection method for the bearing with cage fault.

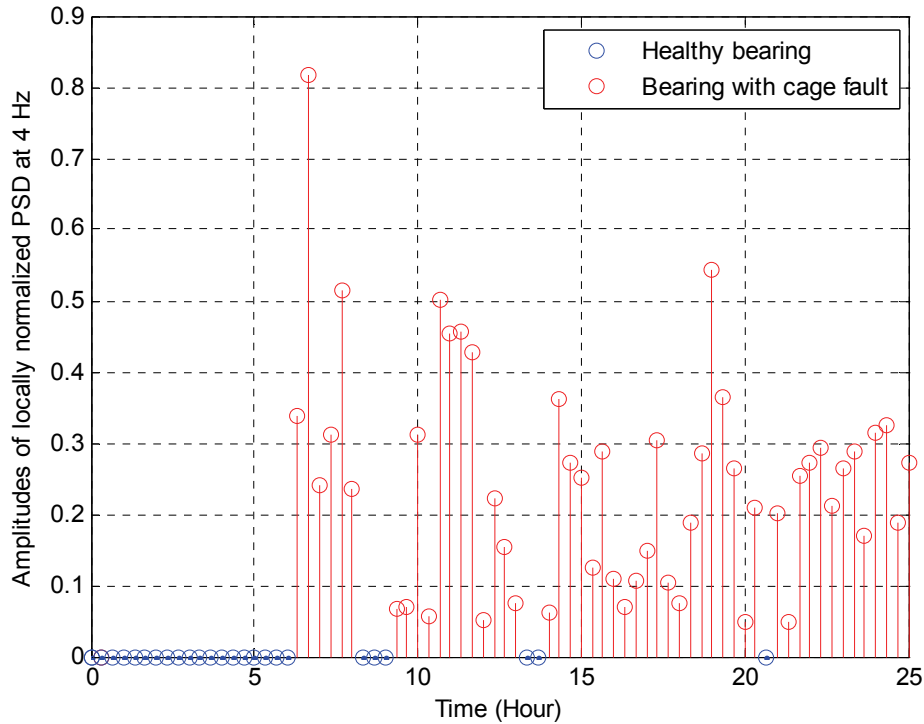


Fig. 6.8: Amplitudes of the locally normalized PSD at the bearing cage fault characteristic frequency of 4 Hz during the 25-hour experiment.

The proposed impulse detection method was also applied to determine whether there is a signature of the bearing cage fault in the PSD of the estimated shaft rotating frequency signal during the entire 25-hour experiment. The result is given in Fig. 6.8. It shows that the signature of the bearing cage fault appeared from the 6<sup>th</sup> hour of the experiment. The fault signature indicates a degradation of the bearing cage and maintenance should be taken immediately. Since there was no maintenance taken after the 6<sup>th</sup> hour of the experiment, the bearing was damaged and the wind turbine was stopped at the 25<sup>th</sup> hour of the experiment by the protection system.

To illustrate the advantage of using the demodulation methods for wind turbine bearing fault detection. The standard PSD and 1P-invariant PSD of the raw stator current measurements are plotted in Figs. 6.8 and 6.9, respectively. Based on Table 6.1 and the shaft rotating frequency, the excitations of bearing cage defect should appear at about  $63 \pm 4 \cdot n$  Hz in Fig. 6.9, where  $n = 1, 2, \dots$ . However, because of the high magnitude of the stator current fundamental-frequency component and the variable shaft rotating frequency, the excitations generated by the bearing fault are totally masked by the stator current fundamental-frequency component in the standard PSD spectrum and, therefore, cannot be detected by using the standard PSD method. In Fig. 6.10, the variable shaft rotating frequency was converted to a constant value of 10 Hz in the 1P-invariant PSD method. The excitations due to the bearing cage defect should appear at  $60 \pm 4 \cdot n$  Hz, where  $n = 1, 2, \dots$ . However, these excitations are masked by the subbands of the

fundamental-frequency component due to it's the high magnitude. It failed to detect the bearing fault for the direct-drive PMSG wind turbine by using the stator current measurements directly.

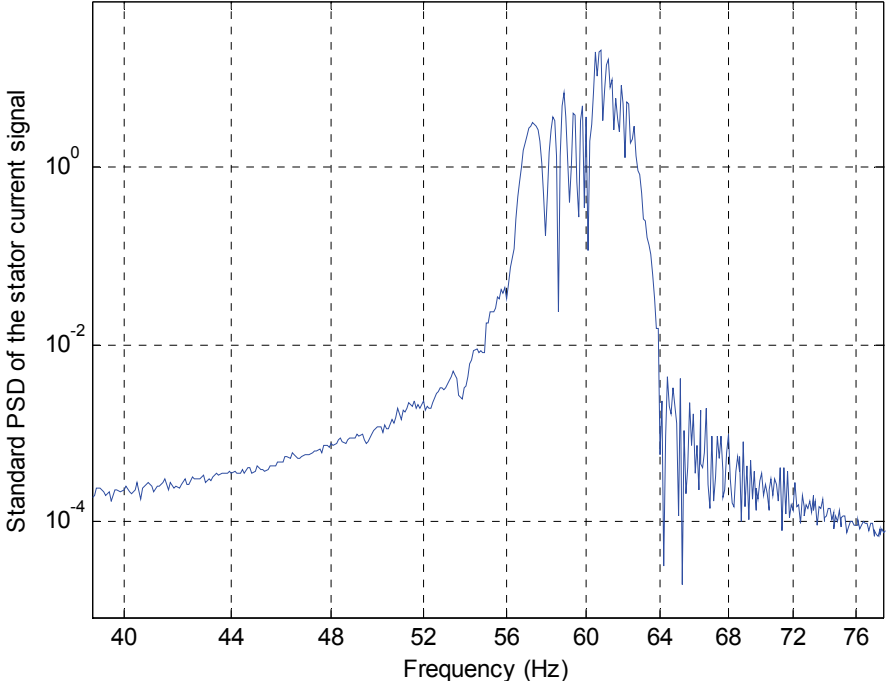


Fig. 6.9: The standard PSD of the stator current measurements in the bearing fault case.

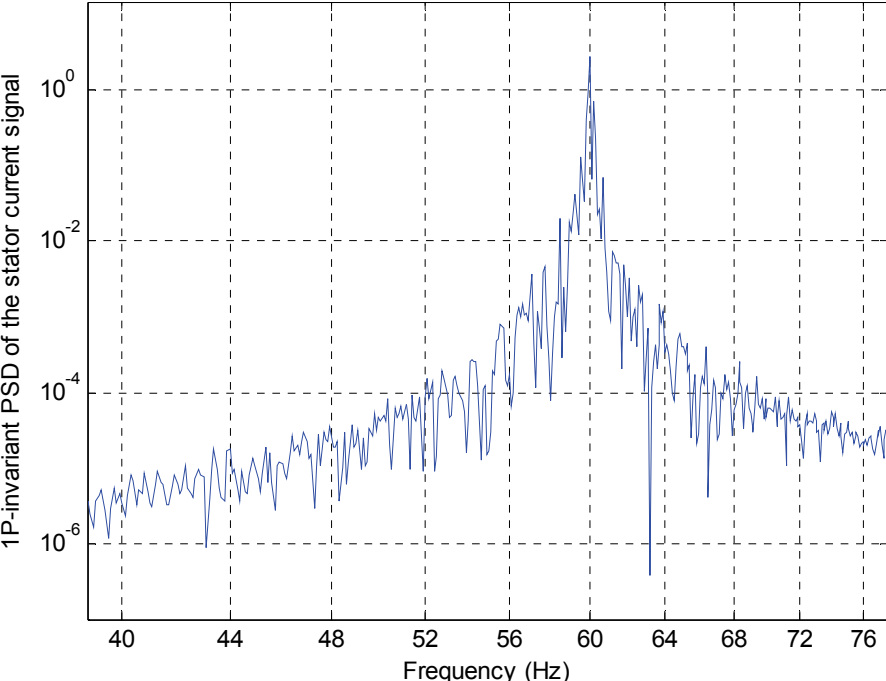


Fig. 6.10: The 1P-invariant PSD of the stator current measurements in the bearing fault case.

### 6.2.3 WTG with an Out-Race Fault

An outer-race fault was generated artificially for a testing bearing, as illustrated in Fig. 6.11. The healthy bearing and the bearing with an outer-race fault were installed in the WTG and tested, respectively. The length of the stator current record in each case was 50 seconds.



Fig. 6.11: The testing bearing with an outer-race fault.

Fig. 6.12 compares the 1P-invariant PSDs of the estimated shaft frequency signals for the WTG with a faulted bearing and against that with a healthy bearing, where in the 1P-invariant PSD the variable 1P frequency of 6~13 Hz was converted to a constant value of 10 Hz. As shown in Fig. 6.12, an excitation appears at a fixed frequency of 30.8 Hz in the PSD plot of the bearing outer-race fault case. This fault characteristic frequency is the same as the one calculated from (6.2) for the WTG operating with a fixed shaft rotating speed of 10 Hz. Therefore, the excitation at 30.8 Hz in the 1P-invariant PSD of the estimated shaft frequency is an effective signature for the bearing outer-race fault diagnosis.

As shown in Fig. 6.13, the proposed impulse detection method was successfully applied to extract the excitations in the 1P-invariant PSD for bearing outer-race fault diagnosis. The length of the window,  $W$ , was also chosen to be 101. The same third-order median filter as for Fig. 6.7 was used to calculate the threshold. The locally normalized PSD [i.e.,  $R(f)$ ] of the bearing outer-race fault case is plotted in Fig. 6.13, where the threshold was calculated to be 0.054. Fig. 6.13 clearly shows that the proposed impulse detection method successfully detected the excitation at 30.8 Hz corresponding to the bearing out-race fault.

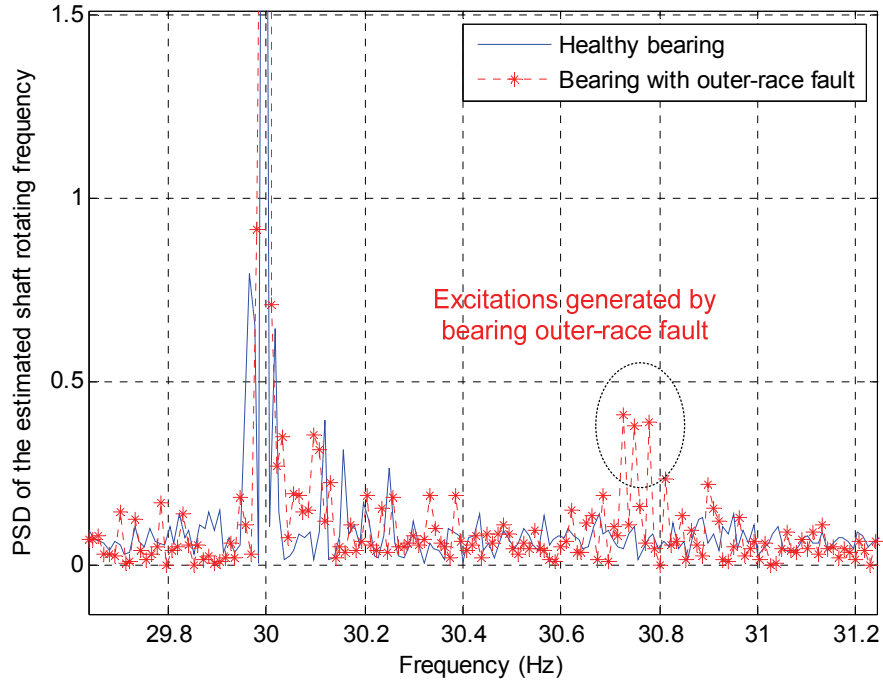


Fig. 6.12: Comparison of the 1P-invariant PSDs of the estimated shaft rotating frequency signals for the WTG with a bearing outer-race fault against that with a healthy bearing.

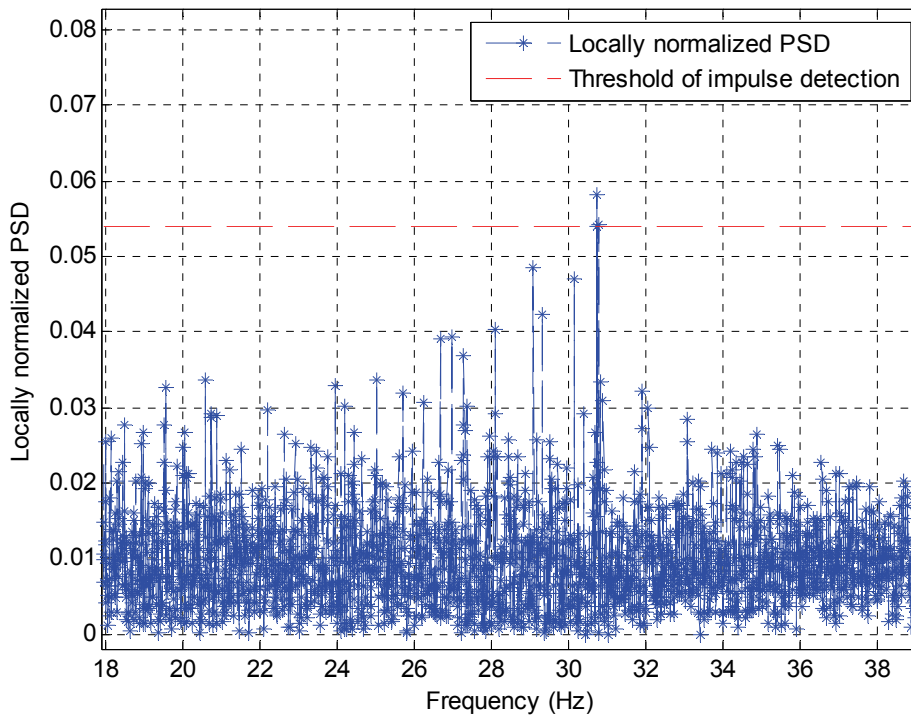


Fig. 6.13: Locally normalized PSD and threshold generated by the impulse detection method for the bearing with an outer-race fault.

### 6.3 Incipient Bearing Fault Detection

An Air Breeze wind turbine with a pretreated bearing (no lubricant) was operated in the wind tunnel of the PI's laboratory. During the experiment, the wind turbine was operated at variable speed conditions with the shaft speed in the range of 500-700 rpm, which is around the maximum shaft speed of this wind turbine. Operating the wind turbine at high speeds also helps accelerating the failure process of the bearing. The experiment took approximately 25 hours.

The proposed wavelet filter-based method was applied to the recorded stator current signals for bearing fault detection. The resulting wavelet-filtered signals represent the energy of the components in the current measurements related to the bearing fault and were used as the signature for incipient bearing fault detection. In each 200-second sampling period, the first  $2^{19}$  samples (approximately 50 second of samples) were used as replication 1; the second  $2^{19}$  samples were used as replication 2; and the third  $2^{19}$  samples were used as replication 3. The use of multiple replications is to demonstrate that the wavelet filter-based fault detection does not depend on when the data was recorded. The results are shown in Fig. 6.14. The energy of the wavelet-filtered stator currents increases during the first 7 hours of the experiment for all three replications. Due to the lack of lubricant, the bearing condition was degrading quickly during this period. From the 8th to 23rd hours, the energy almost stays at the same level. This indicates that the incipient bearing fault has already built up and the bearing was working in a subhealthy condition. During the last one to two hours of the experiment, the energy climbed up and the cage of the bearing was broken at the end of the experiment, as shown in Fig. 6.5; the wind turbine stopped running when the bearing has been broken.

The results of Figs. 6.14 and 6.5 clearly show that the proposed wavelet filter-based method can work effectively to extract the fault signature from the stator current measurements; the resulting fault signature can be used to discover the physical condition of the wind turbine bearing effectively.

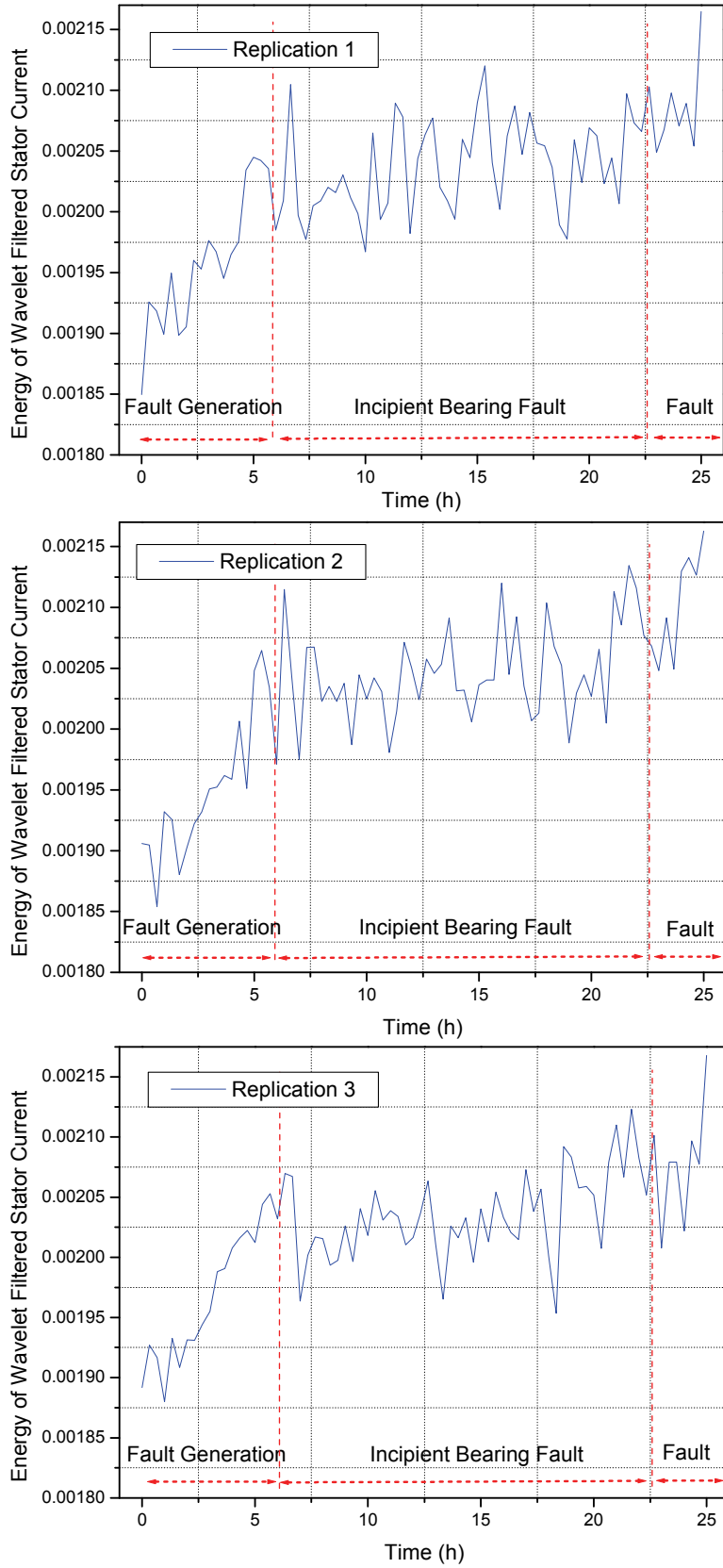


Fig. 6.14: The results of the wavelet-filtered stator current.

## 7. ACCOMPLISHMENTS

### 7.1 Publications

The following peer-reviewed journal and conference proceeding papers have been generated from the findings of this project.

1. X. Gong and W. Qiao, "Imbalance fault detection of direct-drive wind turbines using generator current signals," *IEEE Transactions on Energy Conversion*, vol. 27, no. 2, pp. 468-476, June 2012.
2. X. Gong and W. Qiao, "Current-based online bearing fault diagnosis for direct-drive wind turbines via spectrum analysis and impulse detection," *Proceedings of the 2012 IEEE Symposium on Power Electronics and Machines in Wind Applications (PEMWA 2012)*, Denver, CO, USA, July 16-18, 2012.
3. X. Gong and W. Qiao, "Bearing fault detection for direct-drive wind turbine via stator current spectrum analysis," *Proceedings of the IEEE Energy Conversion Congress and Exposition 2011 (ECCE 2011)*, Phoenix, AZ, USA, Sept. 17-22, 2011, pp. 313-318.
4. X. Gong, W. Qiao, and W. Zhou, "Incipient bearing fault detection via wind generator stator current and wavelet filter," *Proceedings of the 36th Annual Conference of the IEEE Industrial Electronics Society (IECON 2010)*, Phoenix, AZ, USA, Nov. 7-10, 2010, pp. 2615-2620.
5. X. Gong and W. Qiao, "Simulation investigation of wind turbine imbalance faults," *Proceedings of the 2010 International Conference on Power System Technology (POWERCON2010)*, Hangzhou, China, Oct. 24-28, 2010.
6. D.J. Gardels, W. Qiao, and X. Gong, "Simulation studies on imbalance faults of wind turbines," *Proceedings of the IEEE PES General Meeting 2010*, Minneapolis, Minnesota, USA, July 25-29, 2010.
7. X. Gong and W. Qiao, "Current demodulation-based bearing fault diagnosis for direct-drive PMSG wind turbines," *IEEE Transactions on Industrial Electronics*, in review.

The work of the following peer-reviewed conference proceeding paper and Master's thesis has been supported in part by this project.

8. D. Lu and W. Qiao, "Current-based diagnosis for gear tooth breaks in wind turbine gearboxes," *Proceedings of the IEEE Energy Conversion Congress and Exposition 2012 (ECCE 2012)*, Raleigh, NC, USA, Sept. 15-20, 2012.
9. Clark Lacy, "Current-Based Fault Detection for Wind Turbine Generators via Hilbert-Huang Transform," Master's Thesis, Department of Electrical Engineering, University of Nebraska-Lincoln, July 2012.

## 7.2 Presentations

1. W. Qiao, "Current-based online condition monitoring for wind turbines," Center for Research and Education in Wind (CREW), hosted by Colorado State University on Mar. 9, 2012. (Invited presentation).
2. X. Gong and W. Qiao, "Bearing fault detection for direct-drive wind turbine via stator current spectrum analysis," *IEEE Energy Conversion Congress and Exposition 2011*, Phoenix, AZ, USA, Sept. 17-22, 2011.
3. W. Qiao, "Nonintrusive Condition Monitoring for Wind Turbines Using Generator Current Measurements," *2011 Wind Turbine Condition Monitoring Workshop*, Broomfield, CO, September, 2011. (Invited presentation).
4. C. Lacy, X. Gong, and W. Qiao, "Wind Turbine Imbalance Fault Detection Using the Hilbert-Huang Transform," *IEEE Power & Energy Society General Meeting*, July, 2011, Detroit, USA.
5. D. Lu, X. Gong, and W. Qiao, "Stator Current-Based Fault Diagnosis of Wind Turbines Using Optimal ALE & Adaptive Wiener Filter," *IEEE Power & Energy Society General Meeting*, July, 2011, Detroit, USA.
6. X. Gong and W. Qiao, "Wind Turbine Imbalance Fault Detection Using Current Signals," University of Nebraska-Lincoln (UNL) Research Fair, April 13, 2011 and UNL Engineering E-Week, April 15, 2011.
7. W. Qiao, "Incipient bearing fault detection via wind generator stator current and wavelet filter," *36th Annual Conference of the IEEE Industrial Electronics Society*, Phoenix, AZ, USA, Nov. 7-10, 2010.
8. W. Qiao, "Simulation investigation of wind turbine imbalance faults," *2010 International Conference on Power System Technology*, Hangzhou, China, Oct. 24-28, 2010.
9. D. J. Gardels, W. Qiao, and X. Gong, "Simulation studies on imbalance faults of wind turbines," *IEEE Power & Energy Society General Meeting 2010*, Minneapolis, Minnesota, USA, July 25-29, 2010.
10. X. Gong and W. Qiao, "Simulation investigation of wind turbine imbalance faults," *IEEE Power & Energy Society General Meeting*, July 26, 2010.
11. D. Lu and W. Qiao, "Wind tunnel – An advanced platform for wind turbine studies in a laboratory environment," *IEEE Power & Energy Society General Meeting*, July 26, 2010.
12. X. Gong and W. Qiao, "Online Nonintrusive Bearing Fault Detection," University of Nebraska-Lincoln (UNL) Research Fair, April 7, 2010 and UNL Engineering E-Week, April 23, 2010.

## 7.3 Patent

W. Qiao and X. Gong, "System and Method for Wind Turbine Generator Fault Detection Using Generator Current Measurements," U.S. provisional patent 61652396.

## 8. CONCLUSIONS

This project has successfully developed several novel online nonintrusive CMFD technologies for wind turbine. The proposed technologies use only the current measurements that have been used by the control and protection system of a WTG; no additional sensors or data acquisition devices are needed. Current signals are reliable and easily accessible from the ground without intruding on the WTGs that are situated on high towers and installed in remote areas. Therefore, the proposed technologies have great economic benefits and the potential to be adopted by the wind energy industry.

Specifically, this project has analyzed and modeled the effects of faults on the currents of WTGs running in variable rotating speed conditions. A fault induces shaft torque variations in a WTG, which modulate the amplitude and frequency of the current signals. Based on the model and analysis, appropriate frequency and amplitude demodulation methods have been proposed for fault detection for WTGs using only generator current signals. A frequency spectrum analysis method has been applied to discover the excitations at the characteristic frequencies of faults in the demodulated signals. Experimental results have validated the model and the proposed methods for fault detection of direct-drive PMSG wind turbines. The advantages of using frequency and amplitude demodulations of current signals over directly using stator current signals have also been demonstrated by the experimental results.

A novel 1P-invariant PSD method has been developed for imbalance fault detection and quantification of direct-drive wind turbines using only one phase generator stator current signal. The proposed method processes the current or demodulated current signals in a way such that the variable characteristic frequencies of the imbalance faults become constant values in the PSD of the processed signals. Simulation studies have been carried out in a FAST and Simulink combined environment for blade imbalance and aerodynamic asymmetry detection of a 10-kW direct-drive WTG. Experimental studies have been performed in a wind tunnel facility for detection of blade imbalance, bent blades, aged blade, blade defects, and generator magnet damage of a 160-W direct-drive PMSG wind turbine. Both simulation and experimental results have confirmed that the proposed method is effective to detect and quantify various imbalance faults in a variable-speed direct-drive WTG by only using one phase current measured from the generator terminal.

The proposed 1P-invariant PSD method has also been successfully used for detection of various single-point bearing faults in direct-drive PMSG wind turbines, including cage break fault, out-race defect, etc. An impulse detection method has then been designed to extract bearing fault signatures. If an impulse is detected at the characteristic frequency of a bearing fault, an alert will be generated and maintenance of the bearing will be required. Experimental studies for a WTG operating in a wind tunnel have shown that the proposed method can effectively detect various bearing faults for the WTG operating in variable-speed conditions.

The proposed 1P-invariant PSD method is able to clearly identify excitations at the characteristic frequencies of imbalance faults and single-point bearing faults. Therefore, it is sensitive to faults and is immune from interferences near fault characteristic frequencies. Compared to other signal analysis methods, such as wavelet analysis, amplitude demodulation, etc., the proposed method

is less complex and has a lower computational cost and, therefore, is good for online fault detection. Furthermore, the traditional PSD analysis is a well-developed method for fault detection of rotating machines. Therefore, the proposed 1P-invariant PSD method can be easily integrated into existing condition monitoring and fault detection systems used in the wind industry.

A novel wavelet filter-based method has been developed for detecting bearing generalized roughness faults (i.e., incipient bearing faults) for WTGs using stator current measurements. The method decomposes the stator current by using the DWT. The fault-related components in the stator current are located in the low energy part of the decomposed sequence due to the subtle and broad-band features of these components. The low energy points of the decomposed sequence are then identified and added together as the signature of the bearing faults by using the proposed wavelet filter. Experimental data have been obtained from a direct-drive PMSG wind turbine with a developed bearing generalized roughness fault at variable-speed conditions. These data have been used by the proposed method for bearing fault detection successfully.

The PI plans to start up a company in the UNL's Innovation Campus to commercialize the proposed technologies. The final product will be a low-cost, current-based, online, CMFD system that can be easily integrated into commercial WTG systems.

## **9. RECOMMENDATIONS**

Although only validated for small direct-drive wind turbines without gearboxes, the proposed technologies are also applicable for CMFD of large-size wind turbines with and without gearboxes. However, additional investigations, such as validation using field data from operating WTGs, are recommended in order to apply the proposed technologies to those large-size wind turbines. Moreover, in order to facilitate the commercialization of the proposed technologies, further investigations are needed to make them more computational efficient and robust. It is also recommended to combine the proposed technologies with the existing mechanical sensor-based wind turbine CMFD technologies to improve the accuracy and reliability of the wind turbine CMFD systems.

## REFERENCES

- [1] The American Wind Energy Association, "U.S. Wind Industry First Quarter 2011 Market Report," Apr. 2011, [Online]. Available: <http://www.awea.org/learnabout/publications/reports>.
- [2] United States Department of Energy, "20% wind energy by 2030: increasing wind energy's contribution to U.S. electricity supply," Rep. DOE/GO-102008-2567, Jul. 2008.
- [3] B. Lu, Y. Li, X. Wu, and Z. Yang, "A review of recent advances in wind turbine condition monitoring and fault diagnosis," *Proceedings of 2009 IEEE Symposium on Power Electronics and Machines in Wind Applications (PEMWA 2009)*, Lincoln, Nebraska, Jun. 24-26, 2009.
- [4] W. Musial and B. Ram, "Large-scale offshore wind power in the United States: Assessment of opportunities and barriers," Technical Report, National Renewable Energy Laboratory, Sept. 2010, [Online]. Available: <http://www.nrel.gov/wind/pdfs/40745.pdf>
- [5] T.W. Verbruggen, "Wind turbine operation & maintenance based on condition monitoring," Final Report, Energy Research Center of the Netherlands (ECN), April 2003, [Online]. Available: [www.ecn.nl/docs/library/report/2003/c03047.pdf](http://www.ecn.nl/docs/library/report/2003/c03047.pdf)
- [6] Z. Hameed, Y.S. Hong, Y.M. Cho, S.H. Ahn, and C.K. Song, "Condition monitoring and fault detection of wind turbines and related algorithms: A review," *Renewable and Sustainable Energy Reviews*, vol. 13, pp. 1-39, 2009.
- [7] X. Gong and W. Qiao, "Current demodulation-based bearing fault diagnosis for direct-drive PMSG wind turbines," *IEEE Transactions on Industrial Electronics*, in review.
- [8] W. Qiao and X. Gong, "System and Method for Wind Turbine Generator Fault Detection Using Generator Current Measurements," U.S. provisional patent 61652396.
- [9] X. Gong and W. Qiao, "Imbalance fault detection of direct-drive wind turbines using generator current signals," *IEEE Transactions on Energy Conversion*, vol. 27, no. 2, pp. 468-476, June 2012.
- [10] X. Gong and W. Qiao, "Bearing fault detection for direct-drive wind turbine via stator current spectrum analysis," *Proceedings of the IEEE Energy Conversion Congress and Exposition 2011 (ECCE 2011)*, Phoenix, AZ, USA, Sept. 17-22, 2011, pp. 313-318.
- [11] X. Gong, W. Qiao, and W. Zhou, "Incipient bearing fault detection via wind generator stator current and wavelet filter," *Proceedings of the 36th Annual Conference of the IEEE Industrial Electronics Society (IECON 2010)*, Phoenix, AZ, USA, Nov. 7-10, 2010, pp. 2615-2620.
- [12] R. Fadaeinedjad, G. Moschopoulos, and M. Moallem, "The impact of tower shadow, yaw error, and wind shears on power quality in a wind diesel system," *IEEE Transactions on Energy Conversion*, vol. 24, no. 1, pp. 102-111, Mar. 2009.
- [13] R. Ramlau and J. Niebsch, "Imbalance estimation without test masses for wind turbines," *Journal of Solar Energy Engineering*, vol. 131, no. 1, pp. 011010-1 – 011010-7, Feb. 2009.
- [14] J.S. Walker, *A Primer on Wavelets and their Scientific Applications*, Chapman & Hall, 1999.
- [15] D. L. Donoho and I.M. Johnstone, "Adapting to unknown smoothness via wavelet shrinkage," *Journal of American Statistical Association*, vol. 90, pp. 1200-1224, 1995.
- [16] X. Gong and W. Qiao, "Current-based online bearing fault diagnosis for direct-drive wind turbines via spectrum analysis and impulse detection," *Proceedings of the 2012 IEEE Symposium on Power Electronics and Machines in Wind Applications (PEMWA 2012)*, Denver, CO, USA, July 16-18, 2012.

- [17] U.S. Department of Energy, "20% wind energy by 2030: increasing wind energy's contribution to U.S. electricity supply," May 2008, [Online]. Available: <http://www1.eere.energy.gov/windandhydro/pdfs/42864.pdf>
- [18] World Wind Energy Association, "World Wind Energy Report 2010," Apr. 2011, [Online]. Available: [http://www.wwindea.org/home/images/stories/pdfs/worldwindenergyreport2010\\_s.pdf](http://www.wwindea.org/home/images/stories/pdfs/worldwindenergyreport2010_s.pdf)
- [19] W.Q. Jeffries, J.A. Chambers, and D.G. Infield, "Experience with bicoherence of electrical power for condition monitoring of wind turbine blades," *IEEE Proc. on Vision, Image and Signal Processing*, vol. 145, pp. 141-148, 1998.
- [20] T. Bouno, *et al.*, "Failure Forecast Diagnosis of Small Wind Turbine using Acoustic Emission Sensor," *KIEE Int. Trans. Electrical Machinery and Energy Conversion Systems*, vol. 5-B, pp. 78-83, 2005.
- [21] D. J. Lekou, *et al.*, "Emerging Techniques for Health Monitoring of Wind Turbine Gearbox and Bearings," *Proceedings of EWEC 2009, Scientific Track-Operation and Maintenance*, Marseille, France, 2009.
- [22] S. Djurovic, *et al.*, "Condition Monitoring Artifacts for Detecting Winding Faults in Wind Turbine DFIGs," *Proceedings of EWEC 2009, Scientific Track-Wind Turbine Electrical System & Component*, Marseille, France, 2009.
- [23] W. Yang, *et al.*, "Condition monitoring and fault diagnosis of a wind turbine synchronous generator drive train," *IET Renewable Power Generation*, vol. 3, pp. 1-11, Mar. 2009.
- [24] Q. Huang, *et al.*, "Application of wavelet neural networks on vibration fault diagnosis for wind turbine gearbox," *Proceedings of 5th international symposium on Neural Networks: Advances in Neural Networks, Part II*, Beijing, China, 2008.
- [25] C. Chen, *et al.*, "Fault diagnosis for large-scale wind turbine rolling bearing using stress wave and wavelet analysis," *Proceedings of 8th Int. Conf. on Electrical Machines and Systems, 2005 (ICEMS 2005)*, 2005, pp. 2239-2244.
- [26] P. Caselitz and J. Giebhardt, "Rotor condition monitoring for improved operational safety of offshore wind energy converters," *Journal of Solar Energy Engineering*, vol. 127, pp. 253-261, 2005.
- [27] J.J. Christensen, *et al.*, "Remote condition monitoring of vestas turbines," *Proceedings of EWEC 2009*, Marseille, France, 2009.
- [28] N. Weller, "Acceleration enveloping - Higher sensitivity, earlier detection," *Orbit*, pp. 10-19, 2004.
- [29] R.M. Jones, "Enveloping for bearing analysis," *Sound and Vibration*, pp. 10-15, Feb. 1996.
- [30] Z. Wang and Q. Guo, "The Diagnosis Method for Converter Fault of the Variable Speed Wind Turbine Based on the Neural Networks," *Proceedings of 2nd Int. Conf. on Innovative Computing, Information and Control, 2007 (ICICIC 2007)*, 2007, pp. 615-615.
- [31] J. Ribrant and L.M. Bertling, "Survey of failures in wind power systems with focus on Swedish wind power plants during 1997-2005," *IEEE Transactions on Energy Conversion*, vol. 22, no. 1, pp. 167-173, Mar. 2007.
- [32] M. Kumm, H. Klingbeil, and P. Zipf, "An FPGA-based linear all digital phase-locked loop," *IEEE Transactions on Circuits and Systems*, vol. 57, no. 9, pp. 2487-2497, Sept. 2010.
- [33] I. Pitas and A.N. Venetsanopoulos, *Nonlinear Digital Filters: Principles and Applications*, Kluwer Academic Publishers, 1990.

- [34] J.M. Jonkman and M. L. Buhl, *FAST User's Guide*, National Renewable Energy Laboratory, Jul. 2005.
- [35] B.J. Jonkman, *TurbSim User's Guide*. National Renewable Energy Laboratory, 2009.
- [36] D. Jiang, Q. Huang, and L. Hong, "Theoretical and experimental study on wind wheel unbalance for a wind turbine," *Proceedings of the 2009 World Non-Grid-Connected Wind Power and Energy Conference*, Sept. 24–26, 2009.
- [37] Y. Amirat, M.E.H. Benbouzid, B. Bensaker, and R. Wamkeue, "Condition monitoring and fault diagnosis in wind energy conversion systems: a review," *Proceedings of the 2007 IEEE International Electric Machines and Drives Conference*, vol. 2, May 2007, pp. 1434–1439.
- [38] S.A. Saleh and C.R. Moloney, "Development and testing of wavelet packet transform-based detector for ice accretion on wind turbines," *Proceedings of the IEEE Digital Signal Processing Workshop and IEEE Signal Processing Education Workshop*, pp. 72–77, Jan. 2011.
- [39] R. W. Hyers, J. G. McGowan, K. L. Sullivan, J. F. Manwell, and B. C. Syrett, "Condition monitoring and prognosis of utility scale wind turbines," *Energy Materials*, vol. 1, no. 3. pp. 187–203, Sep. 2006.
- [40] T. Burton, D. Sharpe, N. Jenkins, and E. Bossanyi, *Wind Energy Handbook*. New York: Wiley, 2001.
- [41] D.J. Gardels, W. Qiao, and X. Gong, "Simulation studies on imbalance faults of wind turbines," *Proceedings of the IEEE Power & Energy Society General Meeting 2010*, pp. 1–5, July 2010.
- [42] J.F. Manwell, J.G. McGowan, and A.L. Rogers, *Wind Energy Explained*, West Sussex, England: John Wiley & Sons Ltd, 2002.
- [43] J.R. Stack, T.G. Habetler, and R.G. Harley, "Fault classification and fault signature production for rolling element bearings in electric machines," *IEEE Transactions on Industry Applications*, vol. 40, no. 3, pp. 735-739, May/June 2004.
- [44] F. Immovilli, M. Cocconcelli, A. Bellini, and R. Rubini, "Detection of generalized-roughness bearing fault by spectral-kurtosis energy of vibration or current signals," *IEEE Transactions on Industrial Electron.*, vol. 56, no. 11, pp. 4710–4717, Nov. 2009.
- [45] R.R. Schoen, T.G. Habetler, F. Kamran, and R. Bartheld, "Motor bearing damage detection using stator current monitoring," *IEEE Transactions on Industry Applications*, vol. 31, no. 6, pp. 1274–1279, Nov./Dec. 1995.
- [46] M. Blodt, P. Granjon, B. Raison, and G. Rostaing, "Models for bearing damage detection in induction motors using stator current monitoring," *IEEE Transactions on Industrial Electronics*, vol. 55, no. 4, pp. 1813–1822, Apr. 2008.